Monitoring and Predicting Agricultural Droughts for a Water-Limited Subcontinental Region by Integrating a Land Surface Model and Microwave Remote Sensing

Yohei Sawada, Toshio Koike, Eiji Ikoma, and Masaru Kitsuregawa, *Fellow, IEEE*

***Abstract*— Agricultural drought monitoring and prediction technology are urgently needed. We applied an ecohydrological land data assimilation system (LDAS), which can simulate soil moisture and leaf area index (LAI) by data assimilation of microwave brightness temperature into a land surface model (LSM), to monitor and predict agricultural droughts in North Africa. We successfully monitor nationwide crop failures, which are characterized by the declines of the nationwide wheat production, in Morocco, Algeria, and Tunisia using LAI and soil moisture calculated by the LDAS. Our simulated LAI is well correlated with the nationwide wheat production ($r = 0.70$, 0.65, and 0.72 in Morocco, Algeria, and Tunisia, respectively). A general circulation model (GCM)-based seasonal meteorological prediction significantly contributes to accurately predicting LAI and agricultural droughts in 2–3-month lead time. In addition, it is found that initial conditions have an important role in predicting LAI. We demonstrate the capability of our framework to monitor and predict agricultural drought in North Africa. Our proposed framework can contribute to mitigating the negative impact of drought on agriculture in poorly gauged water-limited subcontinental regions.**

***Index Terms*— Drought, land data assimilation, passive microwave remote sensing.**

I. Introduction

MONITORING and predicting severe agricultural droughts are the grand challenges in hydrometeorology. In the twenty-first century, many severe droughts significantly damaged national and regional crop production [1]–[3]. Agricultural drought monitoring and prediction technologies to mitigate drought risks are urgently needed. In this article, we define agricultural drought as the scarcity of root-zone soil moisture and the associated decline of the vegetation growth rate and crop production.

We recommend three requirements which the agricultural drought monitoring and prediction system should have. First, the agricultural drought monitoring system needs to explicitly simulate vegetation states and accurately reproduce regional cereal crop production by a land surface model (LSM). Although agricultural drought has been quantified by the lack of soil water supply in [4] and [5], it is more useful to monitor both root-zone soil moisture and vegetation states simultaneously. Their estimated vegetation indices such as leaf area index (LAI) in the LSM's grid scale should be well correlated with cereal crop production to develop the empirical relationship for the prediction of regional and national crop production. Extreme climate conditions such as precipitation deficiency induce soil moisture deficiency causing plant water stress, decline of vegetation growth, and agricultural drought (see [4], [5]). To deliver appropriate information to decision makers, farmers, pastoralists, and others in the middle of drought, this drought propagation which includes both hydrological and ecological processes should be thoroughly monitored.

Second, the agricultural drought prediction system needs to dynamically forecast the conditions of soil moisture and vegetation in 1–3-month lead time using GCM-based seasonal prediction. Despite the intensive applications of seasonal prediction products to predict crop production, there are significant errors in the skill of GCMs to forecast drought onsets [6]. The applicability of the climate model's seasonal prediction to the simulation of vegetation growth related to cereal crop production should be evaluated. Seasonal prediction of vegetation conditions related to cereal crop production in 1–3-month lead time is beneficial to stakeholders who need to prepare the drought adaptation plan.

Third, the role of initial conditions of vegetation and soil moisture in agricultural drought prediction should be investigated. It is important for drought prediction to obtain an accurate initial condition. The errors in land surface prediction by LSMs arise from uncertainty of three factors: initial land surface conditions (e.g., soil moisture), meteorological forcings (e.g., precipitation), and model structure.

Manuscript received August 2, 2018; revised December 25, 2018, February 25, 2019, and May 31, 2019; accepted June 22, 2019. Date of publication September 24, 2019; date of current version December 27, 2019. This work was supported in part by the Data Integration and Analysis System (DIAS), in part by the Japan Aerospace eXploration Agency (JAXA), and in part by JSPS KAKENHI under Grant JP17K18352 and Grant JP18H03800. *(Corresponding author: Yohei Sawada.)*

Y. Sawada is with the Institute of Engineering Innovation, The University of Tokyo, Tokyo 113-0032, Japan, and also with the Meteorological Research Institute, Japan Meteorological Agency, Tsukuba 305-0052, Japan (e-mail: yohei.sawada@sogo.t.u-tokyo.ac.jp).

T. Koike is with the International Centre for Water Hazard and Risk Management (ICHARM), Tsukuba 300-2621, Japan (e-mail: koike@icharm.org).

E. Ikoma and M. Kitsuregawa are with the Institute of Industrial Science, The University of Tokyo, Tokyo 153-8505, Japan (e-mail: eikoma@tkl.iis.u-tokyo.ac.jp; kitsure@tkl.iis.u-tokyo.ac.jp).

Color versions of one or more of the figures in this article are available online at http://ieeexplore.ieee.org.

Digital Object Identifier 10.1109/TGRS.2019.2927342

Wood and Lettenmaier [7] evaluated the relative importance of initial conditions and meteorological forcings in seasonal hydrological prediction assuming that there are no errors in model structure. They found that initial conditions are more important than meteorological forcings for the streamflow prediction skill for up to 5 months in some cases (see also [8]). The agricultural drought monitoring system should be designed to provide accurate current land surface hydrological and ecological conditions which can be used as initial conditions for LSM-based drought prediction. Even if estimated meteorological forcings were perfect, it might be difficult to dynamically predict vegetation conditions without accurate initial conditions of vegetation and soil moisture. In other words, it is expected that in the medium-term (i.e., 1–3 months) forecast, accurate initial conditions can mitigate the negative effects of the biases in seasonal meteorological prediction. It is important to quantify the predictability of agricultural droughts for an operational application of the agricultural drought prediction system.

Despite a lot of efforts to develop operational drought monitoring systems, to our best knowledge, no operational agricultural drought monitoring and prediction systems meet the requirements stated above. Sheffield *et al.* [9] developed the Princeton African Drought monitor which provides the near-real-time monitoring of soil moisture, evapotranspiration, runoff, and streamflow in Africa by driving the LSM. Although this system monitors the complete set of land hydrological states effectively, its LSM cannot explicitly predict vegetation growth and senescence related to cereal crop production. At this moment, the Princeton African Drought monitor provides the land surface hydrological prediction in 7-day lead, which is not long enough to deliver the effective guidance to prepare agricultural droughts. McNally *et al.* [10] developed the Famine Early Warning Systems Network Land Data Assimilation System (FLDAS). The FLDAS drives multi-LSMs by multi-meteorological forcing data sets to provide the complete set of land hydrological states. However, ecological modeling is not included in their LSM and no seasonal prediction is provided in the FLDAS. In addition, there are few studies which evaluated the role of initial conditions for ecologic and cereal crop prediction in the previous literature.

While drought monitors cited above are based on LSMs, satellite land surface observation is also an important technology which has contributed to monitoring drought. Microwave brightness temperature is sensitive to surface soil moisture and vegetation water content (VWC) [11]–[13], both of which are important variables for agricultural drought monitoring. Microwave land surface observation has an all-weather capacity (i.e., observations are not affected by atmospheric conditions) so that land surface can be monitored frequently. Therefore, the all-weather satellite microwave observations were widely used for drought monitoring [14]. However, root-zone soil moisture cannot be directly observed by satellite observation although water dynamics in root-zone soil is crucially important to monitor and predict agricultural drought. In addition, it is generally difficult to predict the future conditions of soil moisture and vegetation only by the temporally coarse satellite observations. Therefore, it is expected that the complete set of the vegetation condition and the soil moisture's vertical profile is accurately estimated as the temporally continuous data by combining the LSMs and satellite observations for agricultural drought monitoring and prediction system.

An LDAS can effectively combine LSM simulations with observations to obtain the accurate model states and/or LSM's unknown parameters. The LDAS is useful to improve the skill to monitor droughts. In addition, the outputs of LDAS are expected to be appropriate initial conditions for LSM-based prediction. Recently, the LDAS technology was applied to the LSMs which can simultaneously calculate soil moisture and vegetation growth. Ines *et al.* [15] assimilated remotely sensed soil moisture and LAI into an LSM using ensemble Kalman filter (EnKF) to update model state variables and improve the simulation of maize yields. Liu *et al.* [16] assimilated active and passive microwave observations into an LSM and provided a proof-of-concept synthetic experiment to demonstrate the potential of assimilating both active and passive microwave observations in the LDAS to accurately simulate soil moisture and biomass in a rain-fed soybean agricultural system. Barbu *et al.* [17] simultaneously assimilated remotely sensed soil moisture and LAI observations into an LSM and demonstrated the possibility to improve the skill to monitor drought using the LDAS. Sawada and Koike [18] and Sawada *et al.* [19] assimilated passive microwave brightness temperatures observed by Advanced Microwave Scanning Radiometer for Earth Observing System (AMSR-E) and AMSR2, which are sensitive to both surface soil moisture and VWC, into an LSM to improve the skill to simulate both soil moisture and vegetation dynamics. These ecohydrological LDASs which can simultaneously estimate soil moisture and vegetation dynamics (i.e., LAI) related to cereal crop production are promising tools to monitor and predict agricultural droughts.

In this article, we drove the LDAS using observed and predicted meteorological forcings to monitor and predict agricultural droughts. Our objectives are to answer the following questions: 1) can the LDAS reproduce the nationwide crop production of the water-limited subcontinental region? 2) is the state-of-the-art GCM seasonal prediction useful to predict vegetation dynamics and agricultural droughts? and 3) how important are initial conditions to predict vegetation conditions during agricultural droughts compared with meteorological forcing uncertainties?

II. Methods and Materials

A. Coupled Land and Vegetation Data Assimilation System (CLVDAS)

The CLVDAS [18], [19] has been developed to improve the skill of an LSM to simultaneously simulate soil moisture and vegetation dynamics. The LSM of the CLVDAS, EcoHydro-SiB [18], can simultaneously simulate surface soil moisture, root-zone soil moistures, and vegetation states. In a microwave band, the permittivity of liquid water is much higher than that of dry matter. Emissivity in the microwave region strongly depends on soil wetness and VWC so that passive microwave brightness temperatures, surface physical

temperatures multiplied by emissivity, in C- and X-bands are sensitive to liquid water in soil and vegetation (see [11]–[13], [20]–[22]). The all-weather capability of microwave remote sensing to observe terrestrial water and vegetation is useful to be assimilated to improve the skill of an LSM. Using a radiative transfer model (RTM) as an observation operator, the CLVDAS can assimilate passive microwave brightness temperatures observed by AMSR-E and AMSR2 into the LSM. The particle filter (PF) data assimilation method can improve the skill of the LSM to simulate surface soil moisture, root-zone soil moisture, and LAI by using the relationships between state variables from ensemble simulations.

1) Land Surface Model: EcoHydro-SiB: EcoHydro-SiB is the LSM of the CLVDAS. EcoHydro-SiB solves vertical interlayer water flows using a 1-D Richards equation [23]

$$\frac{\partial \theta(z,t)}{\partial t} = -\frac{\partial q_{\text{vertical}}}{\partial z} + r(z,t) \tag{1}$$

$$q_{\text{vertical}} = -K(\theta, z)\left[\frac{\partial \psi(\theta)}{\partial z} - 1\right] \tag{2}$$

where t is the time, z is the distance from the surface with positive values increasing vertically downwards (m), $\theta(z,t)$ is the volumetric water content (m^3/m^3), $r(z,t)$ is the source or sink by evaporation and transpiration, q_{vertical} is the soil moisture flux in the vertical direction ($m^3 s^{-1} m^{-2}$), $\psi(\theta)$ is the capillary suction (m), and $K(\theta, z)$ is the hydraulic conductivity (m/s). Capillary suction and hydraulic conductivity are calculated by the van Genuchten's water retention model [24]

$$\psi(\theta) = \frac{1}{\alpha}(S^{1/m})^{1/n} \tag{3}$$

$$K(\theta,z)/K_s(z) = S^{1/2}[1-(1-S^{1/m})^m]^2 \tag{4}$$

$$S = (\theta - \theta_r)/(\theta_s - \theta_r) \tag{5}$$

$$m = 1 - 1/n \tag{6}$$

where K_s is the saturated hydraulic conductivity (m/s), θ_r is the residual water content (m^3/m^3), and θ_s is the saturation water content or porosity (m^3/m^3). α and n are the model parameters.

EcoHydro-SiB estimates vegetation growth and senescence. In the grassland and cropland case, carbon-pool dynamics are modeled by the following equations:

$$\frac{dC_{\text{leaf}}}{dt} = a_{\text{leaf}}\ \text{NPP} - (d_{\text{leaf}} + \gamma + \lambda)C_{\text{leaf}} \tag{7}$$

$$\frac{dC_{\text{root}}}{dt} = a_{\text{root}}\ \text{NPP} - d_{\text{root}}C_{\text{root}} \tag{8}$$

where C_{leaf} and C_{root} are the carbon pools of leaves and roots, respectively [kg/m^2], a_{leaf} and a_{root} are the carbon allocation fractions of leaves and roots, respectively, and $a_{\text{leaf}} + a_{\text{root}} = 1$. NPP is the net primary production (mol m^{-2} s^{-1}), d_{leaf} and d_{root} are the normal turnover rates of leaves and roots, respectively, and γ and λ are the water- and temperature-related stress factors for leaves, respectively. NPP is calculated by the SiB2 photosynthesis-conductance model [25]. NPP obtained by photosynthesis is allocated into aboveground (C_{leaf}) and belowground C_{root} biomass by the carbon allocation fractions (a_{leaf} and a_{root}). Our carbon allocation fractions are calculated following the method of [26]. Both aboveground biomass and belowground biomass are decreased by the normal turnover. In addition, the aboveground biomass is decreased if the water-related and/or temperature-related stress exists.

The water-related stress factor is derived from the vertical distribution of soil moisture following the method of [27]:

$$\beta_T(i) = \min\left[1, \max\left(0, \frac{\theta_i - \theta_w}{\theta_o - \theta_w}\right)\right] \tag{9}$$

$$\beta_{\text{TOT}} = \sum_{i=1}^{N} \beta_T(i) \times [Y(\Delta z_i \times i) - Y(\Delta z_i \times (i-1))] \tag{10}$$

$$Y(d) = 1 - B^d \tag{11}$$

where β_T (i) is the Soil Moisture Index (SMI) of the ith soil layer, θ_i is the volumetric soil moisture of the ith soil layer, θ_w is the wilting point, and θ_o is the point of stress onset. To obtain θ_w and θ_o, we specify the corresponding suction value and inversely solve (3) and (5). β_{TOT} is calculated by aggregating the SMI in the soil layers, weighted by the root biomass fraction, Y, as in the model of Jackson *et al.* [28] given by (11). N is the number of soil layers, and Δz_i is the depth of each. $Y(d)$ is the cumulative root fraction from the surface to depth d (cm), and B is an empirical parameter that is <1. Please note that a root zone is not set to a specific single soil layer in the EcoHydro-SiB. The contributions of soil moisture in each soil layer to vegetation dynamics are calculated using the cumulative root fraction function. The water-related stress factor, γ, is calculated by

$$\gamma = \gamma_{\max}(1 - \beta_{\text{TOT}})^4 \tag{12}$$

where $\gamma_{\max}$ is the maximum stress loss (see [27]).

EcoHydro-SiB uses the empirical linear relationship between a carbon pool of leaves and LAI suggested by Calvet *et al.* [29]

$$\text{LAI} = \text{SLA} \times C_{\text{leaf}} \tag{13}$$

where SLA is the specific leaf area that indicates leaf thickness (m^2/kg). Passive microwave observations are sensitive to VWC, and LAI cannot directly be observed by microwave remote sensing. Therefore, it is necessary that LAI is converted to VWC in order to improve the skill to simulate LAI by assimilating microwave signals. Paloscia and Pampaloni [20] proposed the empirical relationship between LAI and VWC

$$\text{VWC} = \exp\left(\frac{\text{LAI}}{y}\right) - 1. \tag{14}$$

This relationship has been validated in the previous literature by using *in situ* observation data (see [13]). It has been found that (14) can be applied to the VWC retrieval from microwave brightness temperature in a semiarid region [22]. However, there is the uncertainty in parameter y, which depends on the structure of vegetation, and we chose the value proposed originally by [20] (=3.3). This value has also been used by the previous studies on CLVDAS [19], [20].We used (14) to calculate VWC which is one of the input variables in the RTM (see the following).

Soil hydraulic parameters (K_s, θ_s, α, n,) are retrieved from a soil database (see Section II-B). The other parameters related

to vegetation dynamics such as d_{leaf}, d_{root}, γ_{max}, θ_w, θ_o, and *SLA* are retrieved based on [27] (see also [5, Table 1]).

In each timestep, the original SiB2 submodels of aerodynamics and phosynthesis conductance [24] are first driven to obtain the water source term $r(z,t)$ (i.e., transpiration and evaporation), NPP, and the other heat fluxes. Then, stress factors are calculated by solving (9)–(12) with a soil moisture vertical profile at the previous timestep. (Note that how to calculate the temperature stress factor is omitted in this article since the temperature stress is not important in our study area.) The carbon allocation fractions are also calculated. By using NPP, stress factors, allocation fractions, and normal turnover rates, we solve (7) and (8) by the forward Eular method and update the carbon biomass. The soil moisture state is also updated by numerically solving (1)–(6) with the water source term $r(z,t)$ which has been calculated by the SiB2 submodel [24]. The complete description of the LSM can be found in [18] and [19].

2) Radiative Transfer Model: To directly assimilate brightness temperatures into the model instead of assimilating derived soil moisture and vegetation products, an RTM is needed to convert the land surface conditions to microwave brightness temperatures. The inputs of the RTM are surface soil moisture, surface soil temperature, canopy temperature, and the VWC. All of them are calculated by the LSM, EcoHydro-SiB.

The microwave radiative transfer of a land surface and a vegetation canopy is calculated by the omega-tau model proposed by Mo *et al.* [30]:

$$T_b^{p.f} = T_{bs}^{p,f}\exp(-\tau_c) + (1-\omega_c)T_c(1-\exp(-\tau_c)) + R_{p,f}(1-\omega_c)T_c(1-\exp(-\tau_c))\exp(-\tau_c) \quad (15)$$

where $T_b^{p,f}$ is the brightness temperature at radiometer level (note that we neglect atmospheric contributions), $T_{bs}^{p,f}$ is the brightness temperature at ground level $T_{bs}^{p,f} = (1 - R_{p,f})T_s$, T_s and T_c are the physical land surface and canopy temperatures, respectively, ω_c is the single scattering albedo of the canopy, $R_{p,f}$ is the reflectivity of the land surface, and subscript p and f indicates the polarization (vertical or horizontal), and frequency, respectively. τ_c is the vegetation optical depth (VOD), which is calculated using

$$\tau_c = \frac{b'\lambda_c^x \text{VWC}}{\cos\theta} \quad (16)$$

where b' is the vegetation parameter that does not depend on wavelength (λ_c), x is a parameter that shows a dependence on wavelength (in shorter wavelength, microwave is easier to be attenuated by the vegetation water content), and θ is the incident angle. Equation (16) relates the vegetation dynamics calculated by the LSM with microwave brightness temperature. This linear relationship between VOD and VWC was found by [31]

Land surface emissivity ($= 1 - R_{p,f}$) is calculated by an advanced integral equation model (AIEM) with the incorporation of a shadowing effect [32]. Since the AIEM calculates the dielectric constant of the soil–water mixture, land surface emissivity is the function of surface soil moisture. This part of the RTM relates the surface soil moisture calculated by the LSM with microwave brightness temperature.

3) Data Assimilation: First, the CLVDAS optimizes the unknown parameters of the RTM and EcoHydro-SiB. The parameter optimization module of the CLVDAS searches the optimal parameters by minimizing the cost function defined as a squared difference between simulated and observed brightness temperatures. The shuffled complex evolution method [33] is used as an optimization method. In this module a long time window (>1 year) is chosen, because model parameters do not change in a short period of time. Sawada and Koike [18] provided a detailed description of the parameter optimization scheme. Porosity, hydraulic conductivity, a parameter n of the van Genuchten formula [see (6)], maximum rubisco capacity of top leaf, and correlation length of surface soil roughness were optimized (see [18], [19] for the detail description of these parameters). Sawada and Koike [18] found that simulated passive microwave brightness temperatures were sensitive to these parameters in the semiarid region. Although Sawada and Koike [18] proposed the parameter selection algorithm which can quantitatively estimate the sensitivity of the model parameters to estimated microwave brightness temperatures, this algorithm was not used in this article since it is computationally intensive.

Second, the CLVDAS sequentially adjusts the model states, which are soil moistures of all soil columns and LAI. A PF is used as a data assimilation method. In this module, a short time window (5 days) is chosen. The same observations are used twice in the parameter optimization scheme and PF. Please see Sawada *et al.* [19] for complete descriptions of the data assimilation method.

In comparison with the Kalman filter, including the EnKF, the advantage of the PF is that the prior and posterior distribution of the model state can be represented by Monte Carlo samples and the Gaussian assumption is not needed. The PF is more robust than the KF when the model physics is nonlinear. Although the disadvantage of the PF is its high computational cost, it is feasible to apply the PF to a 1-D LSM. In essence, the PF is simply a Monte Carlo estimation of Bayes' theorem

$$p(x_t|y_{1:t}) \propto p(y_t|x_t)p(x_t|y_{1:t-1}) \quad (17)$$

where $p(x_t|y_{1:t})$ is the probability of the state x at time t, given all observations up to time t. The prior knowledge, $p(x_t|y_{1:t-1})$, based on the model estimation is updated using the likelihood with the new observation at time t, $p(y_t|x_t)$, to obtain the posterior PDF of the state. In the PF, the two factors in the right hand side of (17) are obtained by an ensemble calculation of a numerical model f

$$p(x_t|y_{1:t-1}) \approx \frac{1}{N}\sum_{i=1}^{N}\delta(x_t - f(x_{t-1}^i)) \quad (18)$$

$$p(y_t|x_t) = g(y_t|x_t) \quad (19)$$

where N is the ensemble size, x^i is the realization of the state provided by the ensemble member i, and $\delta()$ is the Direc delta function. The function g is the potential function. In the

CLVDAS, the non-Gaussian potential function is chosen as g

$$g = \exp(-\mathrm{COST}) \tag{20}$$

$$\mathrm{COST} = \frac{1}{N_{\mathrm{obs}}} \sum_{t \in t\,\mathrm{window}} \sum_{p=V,H} \sum_{f=6.9\,\mathrm{GHz},10.7\,\mathrm{GHz},18.7\,\mathrm{GHz}} \frac{\left(T_{b,\mathrm{est}}^{p,f} - T_{b,\mathrm{obs}}^{p,f}\right)^2}{\left(\sigma + \left(T_{b,\mathrm{est}}^{p,f} - T_{b,\mathrm{obs}}^{p,f}\right)^2\right)} \tag{21}$$

where N_{obs} is the total number of satellite scans in the assimilation window, twindow is the temporal length of the assimilation window (5 days in this article), $T_{b,\mathrm{est}}^{p,f}$ and $T_{b,\mathrm{obs}}^{p,f}$ are model-estimated [by (15) and (16)] and satellite-observed brightness temperatures, respectively. We chose the Geman–McClure type estimator [34] for the potential function. Parameter σ is set to 10 in this article. An observation error is not explicitly prescribed in this estimator. We can adaptively reduce the impact of assimilating observations if there are large deviations between initial guess and observation so that this estimator is relatively robust to outliers of observations compared to the Gaussian likelihood function (see in [19, Fig. S1]).

In the CLVDAS, the sampling-importance-resampling (SIR) filter is adopted to implement the analysis update of (17). Normalized weights are evaluated for each ensemble member by

$$w_t^i = \frac{p\left(y_t | x_t^i\right)}{\sum_{i=1}^{S} p\left(y_t | x_t^i\right)}. \tag{22}$$

Then, the posterior is

$$p(x_t | y_{1:t}) \approx \frac{1}{N} \sum_{i=1}^{N} w_t^i \delta\left(x_t - f\left(x_{t-1}^i\right)\right). \tag{23}$$

Ensemble members which simulate microwave brightness temperature more accurately [smaller COST in (21)] get larger weights. The posterior is generated by resampling the ensemble members according to their weights. In the resampling step, the ensemble members with larger weights are sampled more frequently than those with smaller weights. In addition to this resampling step, the generic selection algorithm is adopted to reject ensemble members which do not reproduce observations very well before the resampling step. To prevent the degeneracy phenomenon, in which all but one ensemble member have negligible weights, we add the fluctuation to the state variables of each ensemble member after the resampling process. See Sawada *et al.* [19] for details of the implementation of the PF in the CLVDAS.

It should be noted that the state vector, x, includes soil moisture of all soil layers and LAI

$$x_t^i = \begin{bmatrix} \theta_1 \\ \theta_2 \\ \theta_3 \\ . \\ . \\ . \\ . \\ \theta_{rn} \\ LAI \end{bmatrix} \tag{24}$$

where θ_n is the nth soil moisture layer and rn (= 20 in this article) is the total number of soil layers from the top of the soil to the bottom of the root zone. As described above, surface soil moisture θ_1 and LAI are inputs of the RTM and sensitive to passive microwave brightness temperature. By assimilating microwave brightness temperature, we can modify surface soil moisture and LAI in the data assimilation step. Although soil moistures in the other soil layers, $\theta_{2,\ldots\ldots,rn}$ do not directly affect microwave brightness temperature through the radiative transfer process, the dynamics of surface soil moisture and vegetation growth are strongly affected by root-zone soil moisture in the LSM, as discussed above. Therefore, it can be expected that the reasonable correlation between observable variables (i.e., surface soil moisture and vegetation) and unobservable variables (i.e., deeper-layer soil moistures) is sampled by ensemble members so that we can also modify the deeper-layer soil moistures which are not directly observed.

B. Data

To obtain the initial guess of the model's unknown soil and vegetation parameters, the International Satellite Land Surface Climatology Project 2 soil data [35] and the Food and Agricultural Organization global dataset [36] were used.

The observed brightness temperatures are from the AMSR-E L3 product from 2003 to 2010, which can be downloaded at https://gcom-w1.jaxa.jp/auth.html. We resampled the data from a native resolution (0.1°) to a resolution of 0.25° in order to match it to the resolution of the meteorological forcing dataset and the LSM (see below). Brightness temperatures at 6.925, 10.25, and 18.9 GHz were used since they are sensitive to surface soil moisture and vegetation water content with small atmospheric effects (see [37]). Both horizontally and vertically polarized observations were used. We used only descending pass (night scene) data in order to reduce the effects of surface temperature errors. Although the observation of AMSR-E has been stopped, it is expected that the long record of microwave brightness temperature observations is obtained by AMSR2, which may be useful for the future operational applications (see Section IV-D).

To evaluate the skill of the CLVDAS to simulate phenology (i.e., a yearly vegetation cycle), the Global Land Surface Satellite LAI (GLASS LAI) [38] from 2003 to 2010 was used. The data can be downloaded at http://www.glcf.umd.edu/data/lai/. These LAI data are used just to evaluate the skill of our system to simulate LAI and not used as input of the system. The GLASS LAI is generated from Moderate Resolution Imaging Spectroradiometer (MODIS) visible and infrared observations. The native resolution of the GLASS LAI is 1 km, and we resampled it to 0.25°.

The nationwide crop production data for Morocco, Algeria, and Tunisia were downloaded from FAOSTAT (http://www.fao.org/faostat/en/#home) to detect country-scale crop failures. The total wheat production of Morocco, Algeria, and Tunisia from 2003 to 2010 was used. Since the simulated LAI in each pixel cannot directly be compared with this country-scale crop production data, we spatially averaged the simulated LAI to be compared with wheat production.

The relationship between the nationwide crop production and the simulated LAI by the CLVDAS was evaluated.

As observed meteorological forcings to drive the CLVDAS, the Global LDAS (GLDAS) v2.1 data [39], [40] from 2003 to 2010 were used. The GLDAS data can be downloaded at http://disc.sci.gsfc.nasa.gov/hydrology/data-holdings. The GLDAS provides the complete set of meteorological forcings to run LSMs. The meteorological forcing data of the GLDAS have been widely used in the previous studies (see [41]–[45]). The meteorological forcings used in this article are surface pressure, precipitation, surface air temperature, relative humidity, incoming shortwave radiation, incoming longwave radiation, and wind speed. The horizontal resolution of these data is 0.25°. We linearly interpolated the 3-h data into hourly data.

To predict agricultural droughts using the LSM (EcoHydro-SiB), the atmospheric seasonal prediction is needed. The Geophysical Fluid Dynamics Laboratory (GFDL) hindcast product was used. Ensemble hindcasts were generated from 1980 to present by driving the GFDL's coupled ocean-atmospheric model [46]. The hindcasts are initialized at the first day of each month with 12-month lead time. This product provides 12 ensemble forecasts. This hindcast is a member of the North American Multi-Model Ensemble (NMME) [47]. The data can be downloaded at http://data1.gfdl.noaa.gov. We resampled the monthly precipitation data from the native resolution to a resolution of 0.25° using the bilinear interpolation method [48], [49]. To use the GFDL monthly precipitation as the input of the LSM which needs hourly meteorological forcings, we corrected the GLDAS 3-h precipitation to match the GFDL monthly precipitation every month, as done by [45] (see also Section II-D).

C. Study Area

We applied the CLVDAS to North Africa including Morocco, Algeria, and Tunisia (Fig. 2). Wheat is the major cereal product in these three counties. The growing season of wheat in the three counties is from January to May. Although there are the irrigation activities, the rain-fed agriculture is dominant.

D. Agricultural Drought Monitoring and Prediction

The study period was from 2003 to 2010. The spatial and temporal resolutions of the LSM were set to 0.25° and 1 h, respectively. The vertical resolution of the soil column was set to 0.1 m, but the depth of the first surface soil layer was set to 0.05 m, because the microwave land surface emissivity is sensitive to the soil condition at the depth of less than 0.05 m

First, we optimized the unknown parameters of the EcoHydro-SiB. We run the EcoHydro-SiB in the each model grid from 2003 to 2010. Next, we implemented the sequential data assimilation. The data assimilation module of the CLVDAS (see Section II-A) sequentially adjusted soil moistures of the every soil column and LAI every 5 days. We used 256 ensemble members, which are shown to be a sufficiently large ensemble size by [19], and the ensemble mean is shown in this article as the other previous studies did (see [45], [50]). In this article, the simulation with the data assimilation is called reanalysis. On the other hand, the simulation without any sequential data assimilations but with the parameter optimization is called open loop (OL). We also used the result of the simulation with no parameter optimization and no sequential adjustment (NoDA) to discuss how the data assimilation improves our simulation skill.

We validated the skill of the reanalysis to reproduce past agricultural drought events by comparing the model-simulated LAI with the nationwide wheat production data and the satellite-observed LAI. Past agricultural drought events in North Africa were identified by the yearly total wheat production data of Morocco, Algeria, and Tunisia. The wheat production was analyzed in this article since it is highly sensitive to water availability. Then, we evaluated if these country-scale agricultural droughts can be characterized by the negative anomalies of the simulated LAI by the reanalysis in the harvest season (April) assuming our simulated dynamics of LAI is correlated with the nationwide wheat production. We spatially averaged the simulated LAI to be compared with the country-scale wheat production. In addition, we compared the simulated LAI and the satellite observed LAI to validate the skill of the data assimilation to improve the simulation of vegetation dynamics. We discussed how data assimilation improves the skill to simulate vegetation dynamics by comparing the results of the OL and the NoDA with those of the reanalysis.

To discuss the predictability of vegetation dynamics and agricultural droughts, several hindcast experiments were implemented. In these experiments, we assumed that soil moistures and LAI simulated by the reanalysis were the surrogates of the truth. Therefore, the skill of forecast experiments can be evaluated by their deviation from the reanalysis timeseries (smaller deviations mean better forecasts). First, we drove the LSM with the initial conditions from the reanalysis using the observed meteorological forcings [perfect prediction (PP)]. In the PP, we assumed that the perfect initial conditions and the perfect meteorological prediction were available.

Second, we drove the LSM with the initial conditions in the targeted year from the reanalysis using the observed meteorological forcings (i.e., GLDAS) of every year's record from 2003 to 2010 but the targeted year [Ensemble Stream Prediction (ESP); see [7]]. In the ESP, we assumed that the perfect initial conditions were available while there was no skill to predict the future meteorological conditions and forcings to land surfaces. Therefore, the prediction skill of ESP is brought only by the initial condition.

Third, we drove the LSM with the initial conditions from every year's record from 2003 to 2010 using the observed meteorological forcings in the targeted year [reverse ESP (rESP); see [7]]. The initial condition in the targeted year was not used. In the rESP, we assumed that the perfect meteorological prediction was available while there was no information about the initial conditions. The prediction skill of rESP is brought only by the meteorological forcings. By evaluating the skill of the ESP and the rESP, we can discuss the importance of the initial conditions compared with the predicted meteorological forcings for agricultural drought prediction.

TABLE I
SUMMARY OF FORECAST EXPERIMENTS

Names	Initial condition	meteorological forcings
Perfect Prediction (PP)	perfect	perfect
Ensemble Stream Prediction (ESP)	perfect	climatorogy
reverse Ensemble Stream Prediction (rESP)	climatorogy	perfect
Real Prediction (RP)	perfect	GFDL

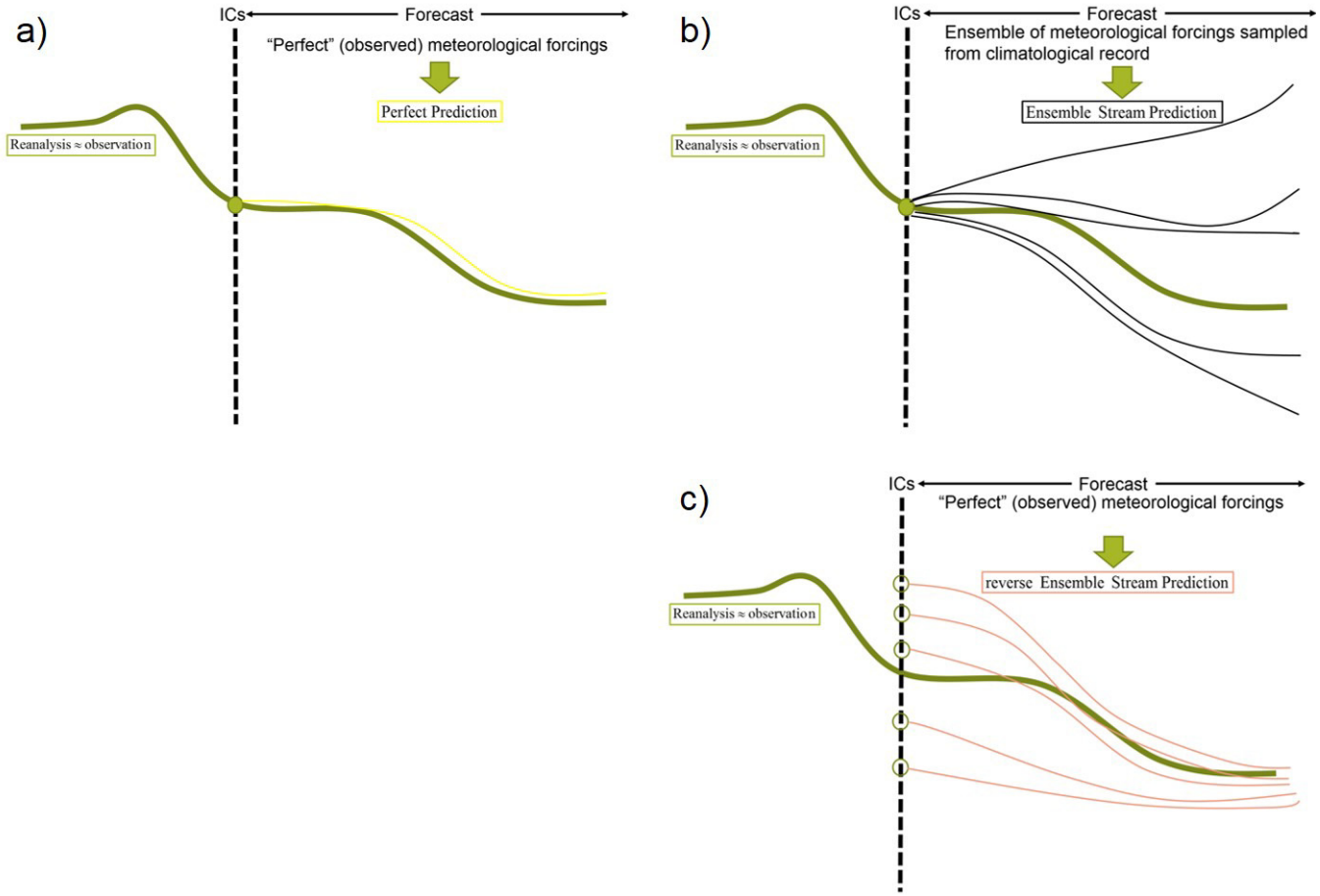

Fig. 1. Schematics of forecast experiments. (a) PP. (b) ESP. (c) rESP. See also Section II and Table I for details of these three experiments.

Finally, we implemented the Real Prediction (RP) in which we drove the LSM using the GFDL seasonal prediction. We used only GFDL monthly precipitation and every forcing but precipitation is from the GLDAS because the temporal resolution of GFDL data is too coarse to drive the LSM, and there are not all necessary meteorological forcings in the GFDL data. We corrected the GLDAS 3-h precipitation to match the GFDL monthly precipitation every month, as done by Sawada and Koike [45].

Table I summarizes the settings of our prediction experiments, and Fig. 1 shows the schematics of the PP, ESP, and rESP. As discussed above, we assumed that the reanalysis can be considered as accurate land surface conditions. Since satellite observations are assimilated into the model-estimated water and vegetation, the reanalysis might be accurate enough to be used as a surrogate of the truth. We specified the time when the forecast was initiated. In the PP and ESP, we sampled the initial conditions from the reanalysis at the forecast initial time [green dots in Fig. 1(a) and (b)]. Then, we started the forecast from this initial condition. In the PP, we drove the LSM by the GLDAS meteorological forcings which are also used to generate the reanalysis. Please note that the results of PP are not identical to the reanalysis since satellite observations are not assimilated in the PP. In the ESP, we also used the observed meteorological forcings (GLDAS). However, we did not use the targeted forecast period's meteorological forcings. Instead, the other year's forcings were used. The ESP prediction is expected to be accurate at the beginning of the forecast period since the forecast is initiated from the accurate observed initial conditions. On the other hand, it is

TABLE II
SCORES OF NODA, OL, AND REANALYSIS TO SIMULATE LAI FROM 2003 TO 2010[a]

	Morocco			Algeria			Tunisia		
	NoDA	OL	reanalysis	NoDA	OL	reanalysis	NoDA	OL	reanalysis
RMSE	0.59	0.32	0.21	0.92	0.39	0.27	0.77	0.30	0.19
R	0.71	0.83	0.89	0.71	0.70	0.80	0.71	0.67	0.80

[a] RMSE: root mean squared error [m^2/m^2]; R: Pearson's correlation coefficient. The simulated and observed LAI are spatially averaged in the area of 33N-35N; 10W-2W (Morocco), 35N-37N; 2W-8E (Algeria), and 34N-37N; 8E-12E (Tunisia). See boxes in Figure 2a.

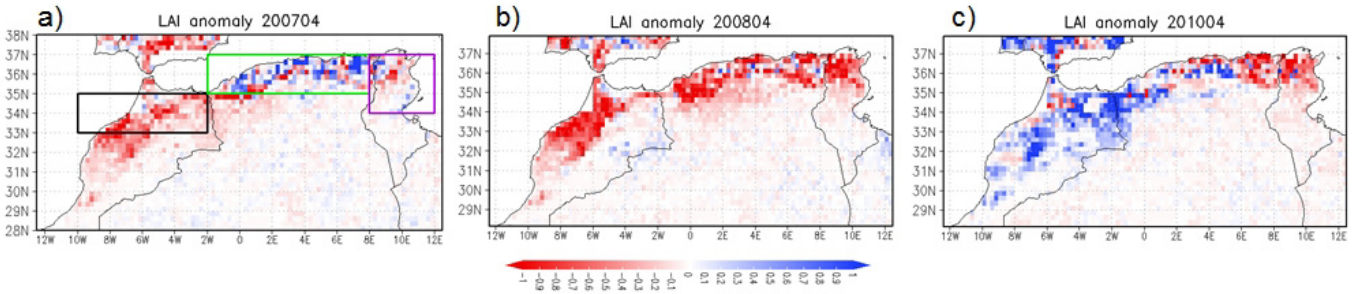

Fig. 2. Anomaly of monthly LAI [m^2/m^2] in the reanalysis averaged in (a) April 2007, (b) April 2008, and (c) April 2010. Black, green, and purple boxes are the areas where we evaluated nationwide statistics of LAI and soil moistures in Morocco, Algeria, and Tunisia, respectively.

expected that the skill is degraded at the end of the forecast period because the meteorological forcings to the LSM spread around the climatology [see black lines in Fig. 1(b)]. In the rESP, the initial conditions are sampled from the reanalysis, but the data in the forecast initial time are not used [see green circles in Fig. 1(c)]. The rESP may have no skill of predicting land surface conditions at the beginning of the forecast period since its initial conditions are significantly biased. On the other hand, it is expected that the skill is improved as the forecast time proceeds since we used the "perfect" meteorological forcings as we used in the PP and the impact of the initial conditions' biases become small [see red lines in Fig. 1(c)].

The drought prediction framework described above was applied to the 2007 Morocco drought. We started the prediction in January and February 2007 and evaluated the skill to simulate vegetation conditions at the end of the growing season (April).

III. RESULTS

We used the estimated LAI in April, which corresponds to the vegetation condition at the end of the growing seasons and the harvest season of wheat crop, as the indicator of agricultural drought in the study area. Fig. 2 shows the anomaly of LAI simulated by the reanalysis in April of 2007, 2008, and 2010 when the declines of wheat production are found in the nationwide crop production data. Fig. 2 indicates that there are large negative anomalies of the reanalysis LAI in the place where the country-scale crop failures are found. Fig. 3 shows the timeseries of the nationwide wheat production and the spatially averaged monthly LAI anomalies in Morocco, Algeria, and Tunisia in April. In 2007, the significant crop failure (i.e., reduction of wheat production) in Morocco can be found in the FAOSTAT data [Fig. 3(a)]. The vegetation degradation in Morocco is simulated by the reanalysis in 2007 [Fig. 2(a)]. The nationwide wheat production data indicate that in 2008, the severe agricultural drought hits all three countries and caused the crop failure in the study region [Fig. 3(a)–(c)]. The reanalysis can reproduce this crop failure in all three countries [Fig. 2(b)]. The wheat production of Tunisia in 2010 was worst in our study period [Fig. 3(c)]. In the reanalysis LAI, the large negative anomaly can be found in Tunisia on April 2010 [Fig. 2(c)]. Correlation coefficients between the anomaly of simulated LAI and the nationwide wheat production in Morocco, Algeria, and Tunisia are 0.70, 0.65, and 0.72, respectively. Overall, the LAI anomaly simulated by the reanalysis can reproduce the country-scale agricultural droughts identified by the nationwide wheat production data.

Fig. 4 shows the mean yearly cycle of LAI in the reanalysis, the OL, the NoDA, and the satellite observation. Temporal means of the satellite observed LAI in Morocco, Algeria, and Tunisia are 0.52, 0.66, and 0.52, respectively. Fig. 4 indicates that the data assimilation has the added value to improve the skill of an LSM to simulate vegetation dynamics. In all three countries, the reanalysis can reproduce the satellite-observed seasonal cycle of LAI better than the NoDA and the OL, which indicates that the parameter optimization and the sequential adjustment of soil moistures and LAI can improve the simulation of vegetation dynamics. Table II shows root-mean-squared error (RMSE) and correlation coefficient (R) between satellite-observed and simulated LAI from 2003 to 2010. Table II indicates that the skill of the reanalysis to reproduce the observed seasonal cycle of LAI is better than those of the OL and the NoDA in all three countries. The parameter optimization reduces RMSE, and the sequential state adjustment further reduces RMSE and increases R.

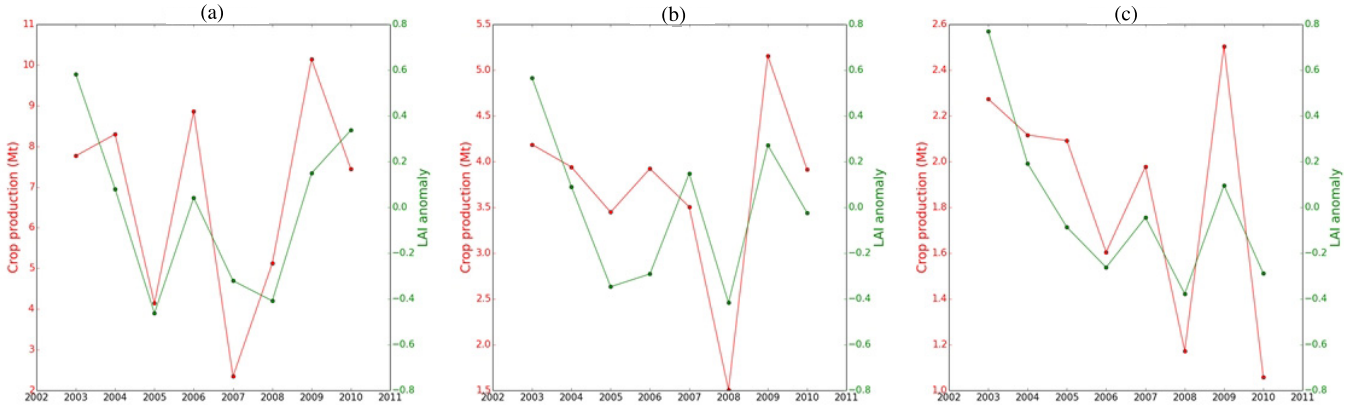

Fig. 3. Timeseries of the nationwide wheat production [Mt] (red) and the anomaly of monthly LAI [m^2/m^2] on April in the reanalysis (green) in (a) Morocco, (b) Algeria, and (c) Tunisia. The anomalies of LAI are spatially averaged in the area of 33N-35N; 10W-2W (Morocco), 35N-37N; 2W-8E (Algeria), and 34N-37N; 8E-12E (Tunisia). See boxes in Fig. 2(a).

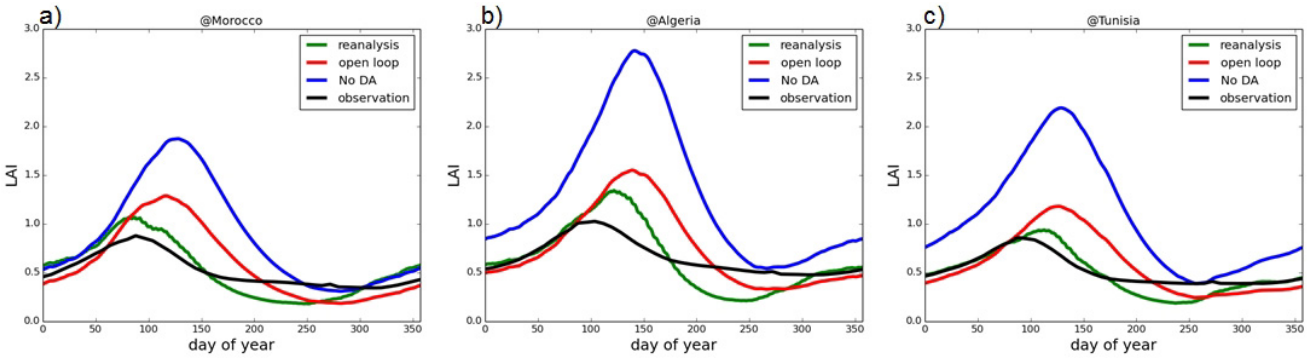

Fig. 4. Climatology of LAI [m^2/m^2] simulated by the reanalysis (green), OL (red), and NoDA (blue) and observed by satellite (black) in (a) Morocco, (b) Algeria, and (c) Tunisia. The climatology of LAI is spatially averaged in the area of 33N-35N; 10W-2W (Morocco), 35N-37N; 2W-8E (Algeria), and 34N-37N; 8E-12E (Tunisia). See boxes in Fig. 2(a).

The simulated LAI by the reanalysis is useful to monitor vegetation dynamics and agricultural droughts. The high correlations between observed and simulated LAI can be found in the coastal region by the pixel-to-pixel comparison (not shown). Since the reanalysis is used as initial conditions for prediction, the data assimilation system can also contribute to predicting agricultural droughts. Please note that the desert pixels are excluded in our analysis [see boxes in Fig. 2(a)] since the variabilities of estimated and observed LAI are extremely small and there may be no agricultural activities in the desert. It should also be mentioned that the meteorological forcings in the desert pixels are unreliable due to the lack of *in situ* observation data there.

One of the advantages of the CLVDAS-based agricultural drought monitoring is that the root-zone soil moistures, which cannot be directly observed by satellite sensors, can be quantitatively estimated by integrating the simulation of the LSM and the land surface observations (i.e., surface soil moisture and vegetation water content). Fig. 5 shows the timeseries of the standardized anomalies of spatially averaged LAI and soil moistures in different soil layers. The standardized anomaly of surface soil moisture (2.5 cm) often recovers from negative to positive variables after precipitation events in the middle of drought. Although satellite observed surface soil moisture products are widely available, it is difficult to develop the early warning system by only surface soil moisture data since the negative anomaly of shallow layers' soil moisture is not persistent in the middle of severe droughts. On the other hand, soil moistures in deeper layers (i.e., below 22.5 cm) and LAI have the persistent negative standardized anomalies for the entire drought period in the five drought events of three North African countries. Root-zone soil moisture and LAI are important variables to be monitored for drought early warning because of their persistency. Figs. 2, 3, and 5 indicate that there are substantial declines of the vegetation growth rate, crop production, and root-zone soil moisture in all identified events so that our identified events meet the definition of agricultural droughts described at the beginning of this article (i.e., the scarcity of root-zone soil moisture and the associated decline of the vegetation growth rate and crop production).

We applied the drought prediction framework described in Section II-D to the 2007 Morocco drought. Fig. 6 shows the timeseries of the simulated LAI by the reanalysis in 2007, PP, ESP, rESP, RP, and climatology calculated from the reanalysis (see Section II-D). The PP can correctly reproduce the LAI timeseries of the reanalysis [Fig. 6(a) and (b)]. The deviation between the PP and the reanalysis indicates the LSM's systematic bias and here it is minimal. The ESP cannot simulate

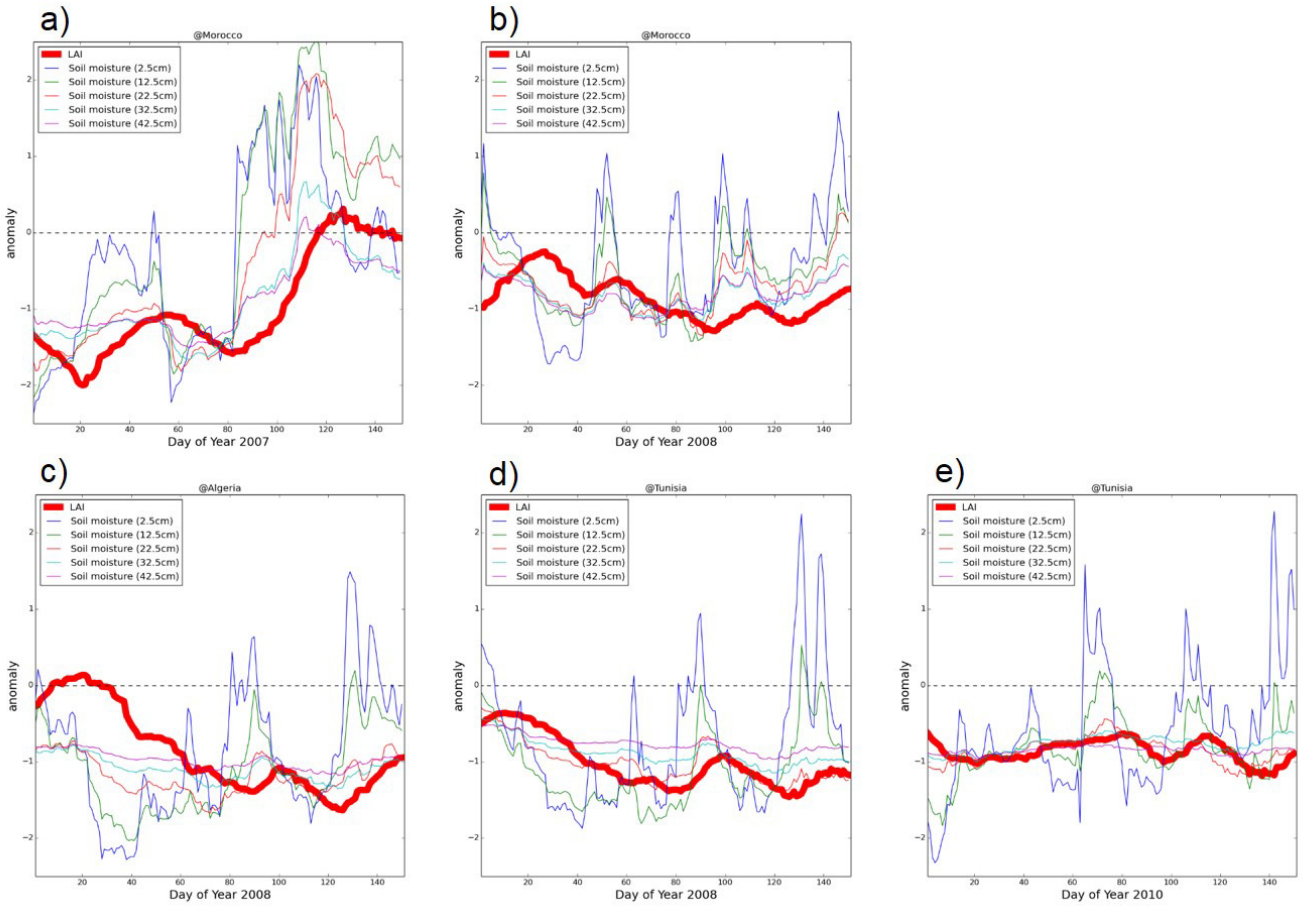

Fig. 5. Standardized anomalies (anomalies divided by standard deviations) of LAI [m^2/m^2] (bold red line) and soil moistures [m^3/m^3] at the depth of 2.5 cm (thinned blue line), 12.5 cm (thinned green line), 22.5 cm (thinned red line), 32.5 cm (thinned cyan line), and 42.5 cm (thinned magenta line) in (a) 2007 Morocco drought, (b) 2008 Morocco drought, (c) 2008 Algeria drought, (d) 2008 Tunisia drought, and (e) 2010 Tunisia drought. The standardized anomalies of LAI and soil moistures are spatially averaged in the area of 33N-35N; 10W-2W (Morocco), 35N-37N; 2W-8E (Algeria), and 34N-37N; 8E-12E (Tunisia). See boxes in Fig. 2(a).

the small LAI at the beginning of the harvest season (April) in the case of predictions starting from both January and February [Fig. 6(c) and (d)]. Even if the perfect initial condition was available, it is difficult to correctly predict vegetation dynamics 2–3 months before without qualified meteorological seasonal prediction. In addition, the rESP fails to simulate the degradation of LAI at the beginning of April [Fig. 6(e) and (f)]. This result indicates that the initial condition, 2–3 months before, has a crucial role in predicting vegetation dynamics. Fig. 6(g) and (h) indicates that the RP can reproduce the negative anomaly of LAI at the beginning of April although the recovery from the severe drought is not correctly simulated. Our simulated LAI is significantly affected just by replacing the precipitation of the GLDAS with that of the GFDL, which indicates that precipitation is more important than the other meteorological forcings to predict agricultural droughts.

In 2007, FAOSTAT shows the average wheat production in Algeria [Fig. 3(b)], and there is the positive anomaly of LAI in the reanalysis [Fig. 2(a)]. The PP correctly simulates this positive anomaly of LAI with the small model bias [Fig. 7(a) and (b)]. In Algeria case, both the ESP and the rESP have the reasonable skills to reproduce the reanalysis LAI [Fig. 7(c)–(f)]. The reanalysis LAI is within the range of one standard deviation of the ensembles of the ESP and the rESP at the beginning of the harvest season (April). The RP can predict the reanalysis LAI although the skill is degraded in the case of the prediction starting from February [Fig. 7(g) and (h)].

In 2007, FAOSTAT shows the average wheat production in Tunisia [Fig. 3(c)], and there is no large anomaly in the reanalysis LAI of Tunisia [Fig. 2(a)]. The PP overestimates LAI due to the model systematic bias in Tunisia [Fig. 8(a) and (b)]. In Table II, the difference of R between the OL and the reanalysis in Tunisia is slightly larger than those in the other two countries. It indicates that the LSM has a relatively large bias in Tunisia since there are the large deviation between the free run of the LSM and the reanalysis which we assumed to be observation. The effect of the model systematic bias decreases as the forecast lead time decreases. This model systematic bias also causes the overestimation of LAI by the ESP [Fig. 8(c) and (d)]. The rESP also significantly overestimates LAI [Fig. 8(e) and (f)]. In 2007, LAI of Tunisia is smaller than climatology from the beginning of January to the beginning of March and it rapidly increases in the middle of March. The rESP overestimates the initial condition of

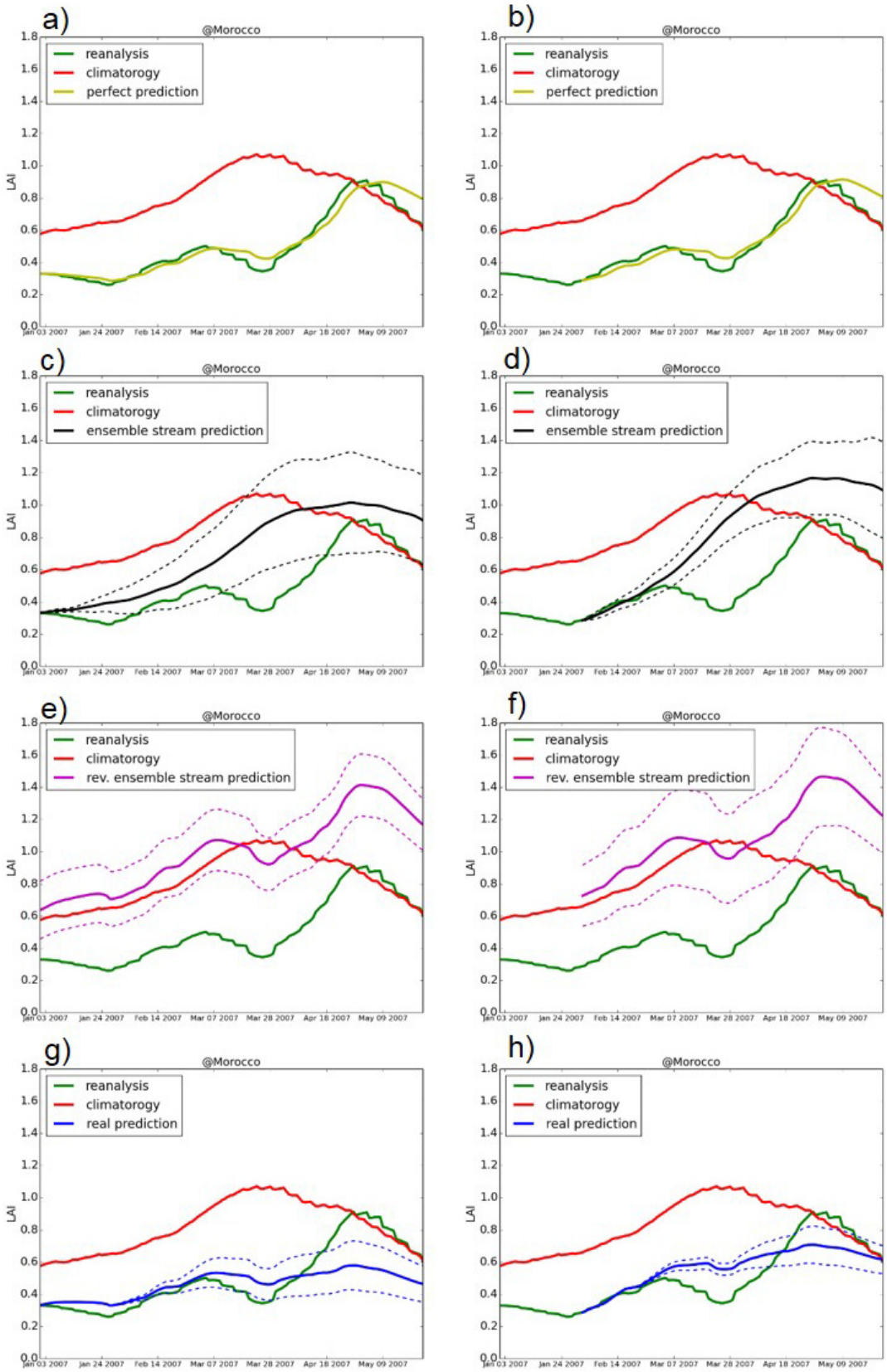

Fig. 6. Timeseries of LAI [m^2/m^2] in the 2007 Morocco drought. Green and red lines are the reanalysis LAI in 2007 and the climatology of LAI calculated from the reanalysis LAI in 2003–2010, respectively. Yellow, black, purple, and blue lines are LAI of PP, ESP, rESP, and RP (see Section II for the definitions), respectively. (a), (c), (e), and (g) Forecast starting from January 1. (b), (d), (f), and (h) Forecast starting from February 1. Bold and dashed lines show the ensemble means and the ranges of one standard deviation, respectively. The simulated LAI is spatially averaged in the area of 33N-35N; 10W-2W. See boxes in Fig. 2(a).

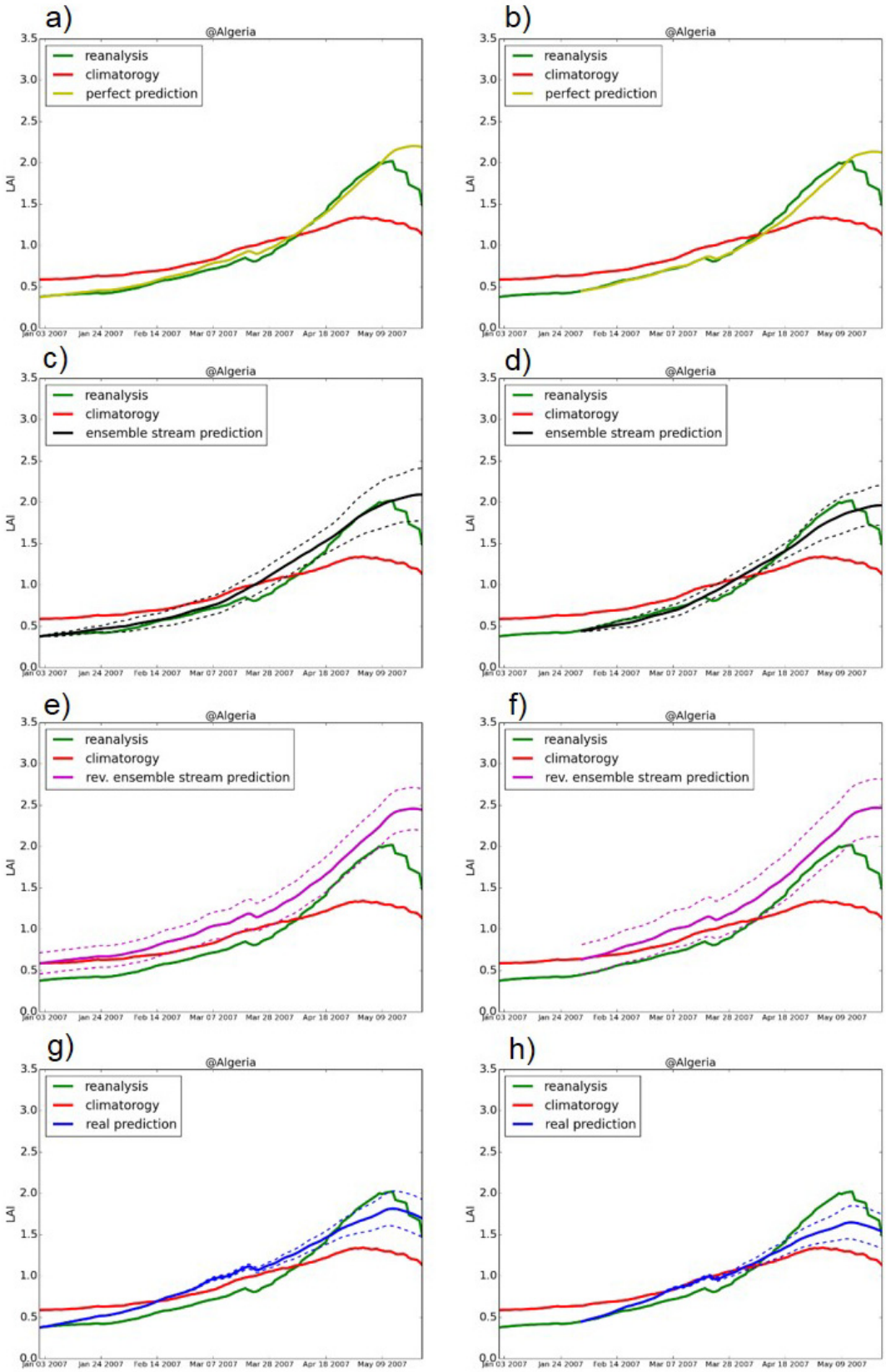

Fig. 7. Timeseries of LAI [m^2/m^2] in the 2007 Algeria drought. Green and red lines are the reanalysis LAI in 2007 and the climatology of LAI calculated from the reanalysis LAI in 2003–2010, respectively. Yellow, black, purple, and blue lines are LAI of PP, ESP, rESP, and RP (see Section II for the definitions), respectively. (a), (c), (e), and (g) Forecast starting from January 1. (b), (d), (f), and (h) Forecast starting from February 1. Bold and dashed lines show the ensemble means and the ranges of one standard deviation, respectively. The simulated LAI is spatially averaged in the area of 35N-37N; 2W-8E. See boxes in Fig. 2(a).

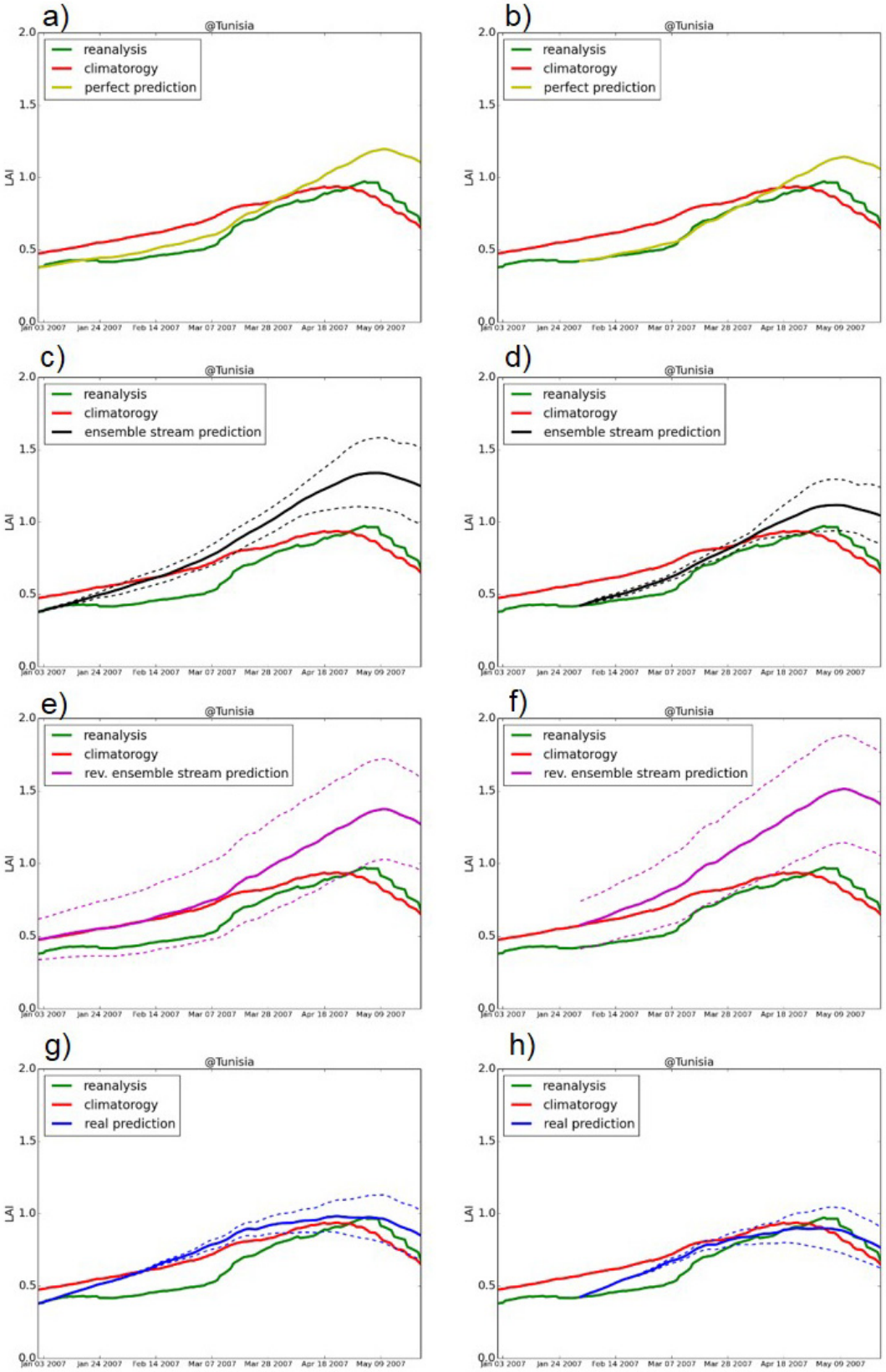

Fig. 8. Timeseries of LAI [m^2/m^2] in the 2007 Tunisia drought. Green and red lines are the reanalysis LAI in 2007 and the climatology of LAI calculated from the reanalysis LAI in 2003–2010, respectively. Yellow, black, purple, and blue lines are LAI of PP, ESP, rESP, and RP (see Section II for the definitions), respectively. (a), (c), (e), and (g) Forecast starting from January 1. (b), (d), (f), and (h) Forecast starting from February 1. Bold and dashed lines show the ensemble means and the ranges of one standard deviation, respectively. The simulated LAI is spatially averaged in the area of 34N-37N; 8E-12E. See boxes in Fig. 2(a).

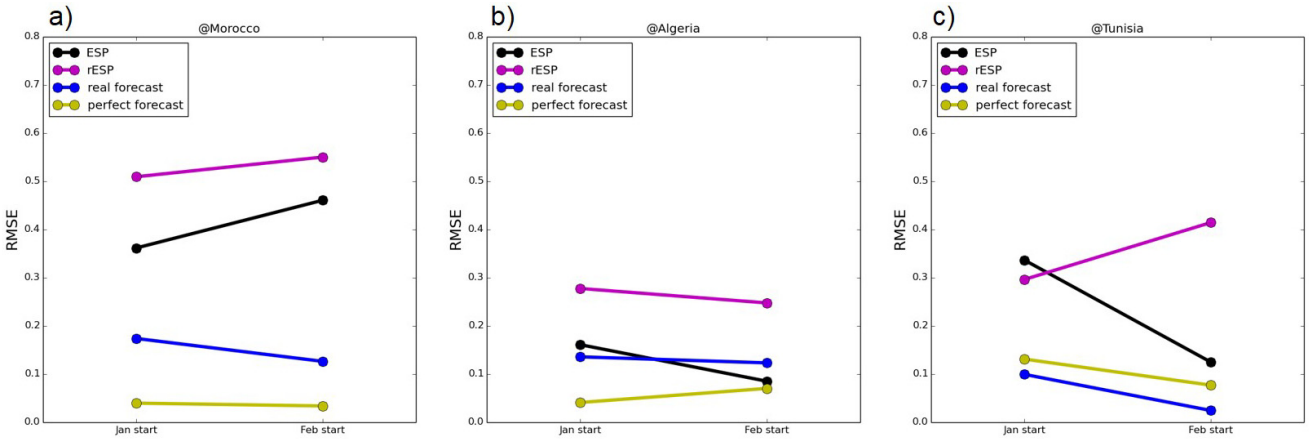

Fig. 9. RMSE between the reanalysis and the predictions in (a) Morocco, (b) Algeria, and (c) Tunisia during April. The predictions include the ESP (black), rESP (purple), RP (blue), and PP (yellow) starting from January 1 to February 1.

LAI and the LAI rapidly increases further in the middle of March. Therefore, the rESP has the tremendous positive bias of simulating LAI in Tunisia. The RP can reproduce the reanalysis LAI even better than the PP. This is because the GFDL prediction underestimates the monthly precipitation, which mitigates the positive bias of simulated LAI shown in the PP. Therefore, it should be noted that the successful LAI prediction by the RP is obtained by the wrong process.

Fig. 9 summarizes the skills of PP, ESP, rESP, and RP. First, the RP outperformed the ESP and the rESP in the every case but the case of the prediction starting from February in Algeria. The state-of-the-art seasonal meteorological prediction is useful for agricultural drought prediction if accurate initial conditions are obtained. Second, the skill of the rESP is worse than that of the ESP in the every case but the case of the prediction starting from January in Tunisia. This result indicates that the initial conditions of soil moisture and LAI have an important role in predicting agricultural droughts in 2–3-month lead time compared with the uncertainties in meteorological forcings.

IV. Discussion

A. Can the LDAS Reproduce the Nationwide Crop Production of the Water-Limited Subcontinental Regions?

This article verifies that our LDAS-based framework is useful to monitor and predict the nationwide crop production and agricultural droughts. We find that our simulated LAI at the end of the growing seasons is well correlated with wheat production and the data assimilation improves the skill of an LSM to reproduce the satellite-derived phenology so that the LDAS can reproduce the nationwide crop production of the water-limited region. Our simulated root-zone soil moisture is also useful to monitor agricultural droughts because of its persistency.

Considering the large footprint size of satellite passive microwave observations, it is difficult to make our current spatial resolution (i.e., 0.25°) finer, which limits the capability of the LDAS-based drought monitoring framework. All variables estimated by the LDAS-based framework should be recognized as the averaged variables in the grids with the coarse resolution and any phenomena whose scales are smaller than the 0.25° cannot be explicitly simulated. The LDAS-based framework cannot directly predict a wide variety of crop yields since regional agricultural activities cannot be explicitly simulated by the LSM with coarse grid sizes. It is also difficult to predict vegetation dynamics and crop failure in a scale smaller than the model grid size. However, the spatiotemporal resolution adopted in this article is appropriate considering the scale of our targeted phenomena and the purpose of our drought monitoring. In general, drought is a climatological phenomenon which has large spatial (larger than 100 km) and temporal (longer than 1 month) scales. Therefore, our drought monitoring system can reasonably resolve drought as a natural phenomenon. In addition, our primary purpose is to provide useful information for stakeholders to consider drought adaptation strategy in national and regional scales, which can be resolved in our system. Note that the existing regional drought monitors also chose the similar spatiotemporal resolutions ([9], [10]).

In the previous literature, statistical models were constructed to estimate the yields of specific regional crops from precipitation and other land surface variables (see [51]). The root-zone soil moisture and LAI simulated by the LDAS-based framework can be used as inputs of the statistical models to predict the yields of the specific crops, which might be useful for local farmers. In addition, the drought severity classification can be made using the outputs of the CLVDAS. The U.S Drought Monitor issues classified drought categories (from D0 to D4) using a wide variety of criteria (see http://droughtmonitor.unl.edu/AboutUs/ClassificationScheme.aspx). The classified drought categories generated from the drought monitoring system might be useful information for local stakeholders.

Although data assimilation substantially improved the skill of the LSM to simulate LAI, there is much room to further improve the skill to simulate vegetation dynamics. The timing of the annual peak of simulated LAI is delayed compared

with that of the satellite-derived LAI. Note that the time lag of the annual peaks between simulated and observed LAI has also been found in the previous studies (see [52]). Although assimilating microwave brightness temperature observations can mitigate this model bias, the parameterization of vegetation growth in its infancy and the die-off in the end of growing season should be improved to completely eliminate this bias. In addition, the optically observed phenology (i.e., LAI) is not completely identical to the phenology derived by microwave signals and the source of the difference between optical and microwave observed vegetation dynamics has not been completely identified [18], [53], [54]. In Algeria and Tunisia, the time lag of the LAI annual peaks between the simulation and the satellite optical observation cannot be completely eliminated by data assimilation because the phenology observed by microwave signals are also delayed compared with that observed by GLASS LAI (not shown). Since our simulated phenology by the reanalysis is constrained to microwave observed phenology, our simulated LAI cannot be completely adjusted to optically observed LAI by data assimilation. In our current LSM, simulated LAI corresponds to vegetation water content one-to-one by (14). We should enable the LSM to separately simulate LAI and vegetation water content in order to reproduce the differences between the optical and microwave vegetation observations.

Please note that there are processes which are important to monitor agricultural droughts but not included in the LSM. Although the declines of crop production detected in this article correspond to the declines of observed precipitation (not shown) and estimated root-zone soil moisture, the decline of agricultural production may be able to occur even if there is no precipitation decline. Agricultural activities can also be damaged by floods, which are not modeled in the current LSM. Political and economic factors sometimes affect agricultural production. In the future operational application, these factors should be carefully considered when the outputs of our system are interpreted.

B. Is the State-of-the-Art GCM Seasonal Prediction Useful to Predict Vegetation Dynamics and Agricultural Droughts?

We revealed that the GCM-based seasonal meteorological prediction is useful to accurately predict LAI and agricultural droughts in 2–3-month lead time. The ensemble mean of ESP, which starts the forecasts from the accurate initial conditions using the observed meteorological forcings of past record, is the "business-as-usual" scenario. If we do not have any information about future atmospheric conditions, it is reasonable to assume climatological atmospheric conditions to forecast the future land surface conditions. In the case of the 2007 Morocco drought, the LAI prediction by the GCM-based seasonal meteorological prediction significantly outperforms the ESP. Our result indicates that the seasonal prediction data set has the benefit to accurately predict the land surface conditions and agricultural droughts. Please note that the error source of our prediction experiments is only precipitation since the other variables of the GCM-based seasonal meteorological prediction are not used in this article.

As Yuan and Wood [6] revealed, the skill of the GCM to predict precipitation is poor in some regions. Although our results are encouraging toward predicting agricultural droughts using the LDAS and the seasonal meteorological prediction, the prediction skill should be thoroughly evaluated in the other regions.

C. How Important Are Initial Conditions to Predict Vegetation Conditions During Agricultural Droughts Compared With Meteorological Forcing Uncertainties?

Following [7], we implemented the ESP and rESP experiments in the framework of agricultural drought prediction to separate the source of the prediction skill into the accuracy of initial conditions and that of meteorological forcings. The ESP assumes that the accurate initial conditions are available while there are no information about the future meteorological conditions. Therefore, the prediction skill of ESP is brought only by the initial condition. On the other hand, the rESP assumes that there are no information about the initial conditions while the perfect meteorological forcings are available. The prediction skill of rESP is brought only by the meteorological forcings.

We concluded that initial conditions are important to predict vegetation conditions during agricultural droughts. In the 2007 Morocco drought, the ESP outperformed the rESP to predict LAI. It reveals that the initial conditions are more important than the meteorological forcings (i.e., seasonal meteorological predictions) to predict agricultural droughts in 2–3-month lead time. Even if the perfect seasonal atmospheric prediction was available, the accurate agricultural drought prediction could not be possible without accurate initial conditions of root-zone soil moisture and LAI. This result encourages to develop a sequential data assimilation system, which improves the drought monitoring and the initial conditions for prediction by combining the numerical simulation and observations up to forecast start time, in order to accurately predict agricultural droughts.

To our knowledge, we evaluated the source of predictability of land surface vegetation conditions in the real-world drought event for the first time. The importance of the initial condition to predict vegetation dynamics may strongly depends on the regional climate. The role of soil moisture's initial conditions found in the water-limited regions cannot be directly applied to wetter regions. More holistic analyses on the predictability of vegetation dynamics should be implemented in the future.

D. Toward the Operational Agricultural Drought Monitoring and Predicting System

Our proposed agricultural monitoring and prediction system can be applied operationally. Fig. 10 shows the proposed agricultural drought monitoring and prediction system which can be operationally applicable to the global water-limited area. Our proposed system supports both drought monitor and prediction functions.

In the drought monitor module [Fig. 10(a)], we generate "reanalysis" land surface soil moisture and LAI, which are used as an initial condition for the drought prediction module.

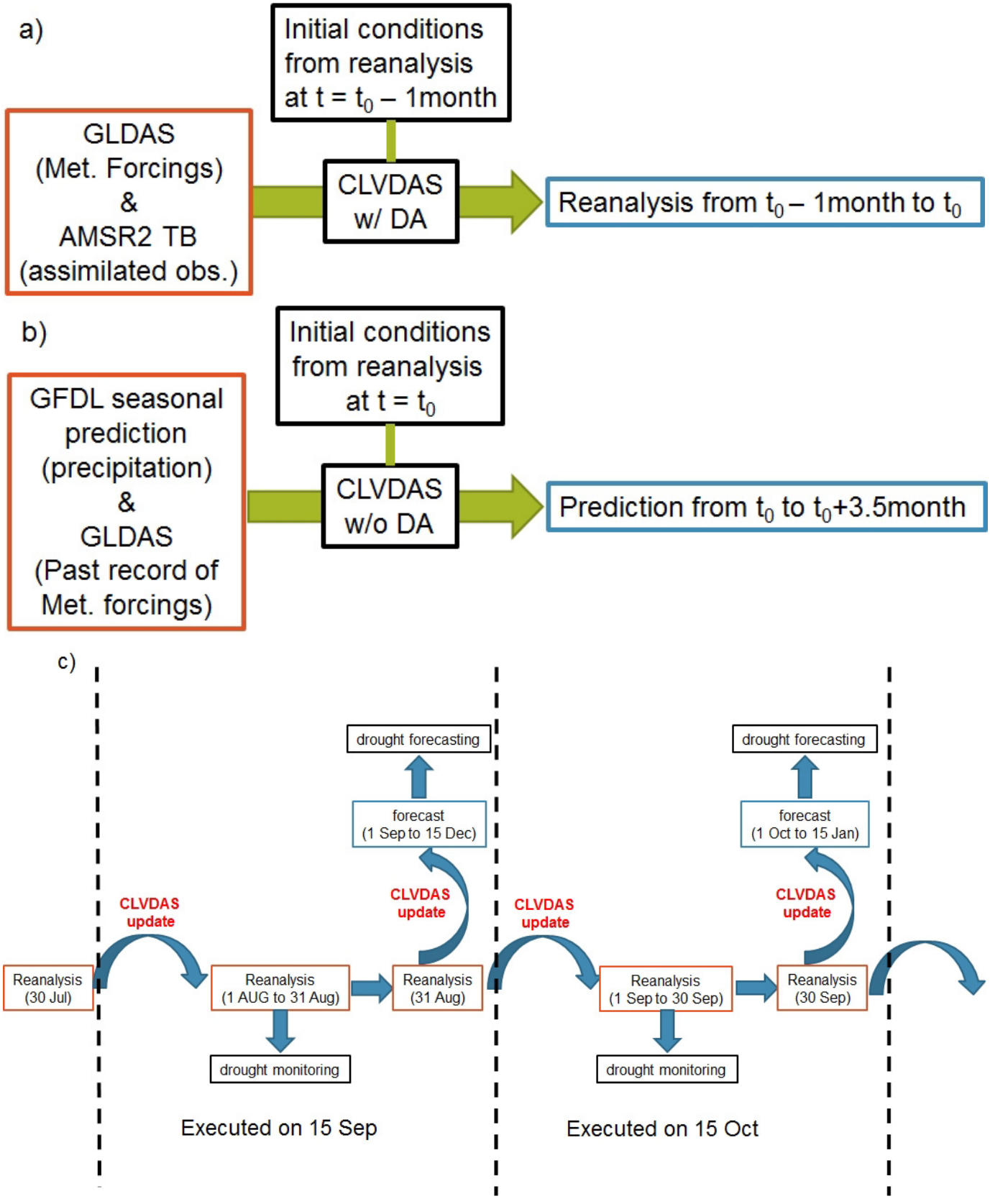

Fig. 10. Schematic of our proposed operational agricultural drought monitoring and prediction system. (a) Drought monitoring module. (b) Drought prediction module. (c) Cycle of monitoring and prediction procedures considering the latency of the input data. See Section IV-D for details.

TABLE III
SUMMARY OF THE DIFFERENCES BETWEEN THIS ARTICLE AND THE EXISTING DROUGHT MONITORS IN AFRICA. BOLD LETTERS SHOW THE ADVANTAGES OF OUR PROPOSED METHOD

	this study	Princeton	FLDAS
Forecast	**Yes (3-month lead)**	Yes (7-day lead)	No
Sequential DA	**Yes (microwave)**	No	No
Estimated land surface variables used for drought monitoring and prediction	Soil Moisture, evapotranspiration, runoff, **Leaf Area Index**	Soil Moisture, Evapotranspiration, runoff, streamflow	Soil Moisture, Evapotranspiration, runoff, streamflow
LSM(s)	EcoHydro-SiB	VIC	VIC, Noah
meteorological forcing dataset	GLDAS (monitoring), GFDL (prediction)	TMPA+NCEP GFS+empirical regressions	RFE2+GDAS, CHIRPS+MERRA-2

We drive the CLVDAS using GLDAS data as observed meteorological forcings and satellite-observed passive microwave brightness temperatures as land surface observation data to be assimilated into the LSM. Although the AMSR-E operational observation was stopped, we can use the observations from its successor, AMSR2 [37]. The other passive microwave satellite observations, such as SMOS and SMAP, can also be used in our system. Since we directly assimilate the brightness temperature (not derived products), assimilating the other passive microwave observation in our framework is straightforward.

In the drought prediction module [Fig. 10(b)], we drive the LSM from the "reanalysis" land surface soil moisture and LAI obtained by the drought monitoring module. We use the GFDL seasonal prediction data to drive the LSM. Replacing the GFDL seasonal prediction dataset with the other seasonal prediction datasets is straightforward. Since the GFDL and other seasonal forecast datasets do not always provide the complete set of meteorological forcing data necessary to run the LSM, some empirical models (see [55]) are needed to prepare the complete meteorological forcings. It is also promising that we use the past record of the GLDAS and the precipitation of the GLDAS is scaled by the GFDL monthly precipitation seasonal forecast to drive the LSM to predict the future land surface conditions. We believe that the ESP is also useful so that the LSM is driven by the past record of the GLDAS meteorological forcings. The PP and rESP were implemented in this article for the research purpose and cannot be operationally done since they need "observations in the future."

Since this drought monitoring and prediction system uses data provided by the other data centers, the latency of the input data should be considered to make our system operational. Satellite microwave brightness temperature observations can be obtained near-real time. The GFDL seasonal prediction is issued every month. The latency of the GLDAS is 1.5 month which is the longest latency in the data sets used in our framework. Optical LAI data are not needed in our framework. Fig. 10(c) shows the schematic illustration of the drought monitoring and prediction cycle. Let us assume that today is September 15. The GLDAS 3-h meteorological forcing dataset from August 1 to August 31 is provided this day. We will download it and drive the CLVDAS using this GLDAS data and AMSR2 satellite observation data to extend our "reanalysis" to 00UTC September 1 for monitoring purpose. The "reanalysis" at 00UTC September 1 is used as an initial condition for the drought prediction module. The GFDL seasonal prediction whose forecast start time is 00UTC September 1 has already been available so that we will drive the LSM using this data to provide the 3.5-month drought prediction from September 1 (3-month prediction from September 15).

E. Comparison With Existing Operational Systems

The drought monitoring and prediction framework developed in this article are suitable to be applied to poorly gauged water-limited subcontinental regions. In previous studies, several drought monitors have already been developed to apply the African region. Here, we compare our newly proposed system with two existing drought monitoring frameworks, the Princeton African Drought monitor [9] and the Famine Early Warning Systems Network LDAS (FLDAS) [10]. Please note that we will focus only on their capability to produce the land surface variables related to drought quantification although they also have the functions to visualize the meteorological datasets which are not made by themselves. The summary of this comparison is shown in Table III.

In the Princeton African Drought monitor, the variable infiltration capacity (VIC) land surface hydrological model [56] is used to provide soil moisture, evapotranspiration, runoff, and streamflow. The real-time simulation is forced by a combination of precipitation from the Tropical Rainfall Measurement Mission (TRMM) Multisatellite Precipitation Analysis (TMPA) [57], temperature and wind speed from the National Centers for Environmental Prediction (NCEP) Global Forecast System (GFS), and the other variables from the empirical model (see [55]). No land surface observations are sequentially assimilated to the VIC in this model update. The VIC is also driven by GFS 7-day forecast to provide the future land surface condition.

In the FLDAS, the VIC and Noah LSM [58] are used to provide soil moisture, evapotranspiration, runoff, and streamflow. The models are driven by a combination of precipitation

from the African Rainfall Estimation version 2.0 (RFE2) [59] and the Climate Hazards group Infrared Precipitation with Stations (CHIRPS) [60] data set, and the other meteorological forcings from National Oceanic and Atmospheric Administration (NOAA) Global Data Assimilation System (GDAS) and Modern Era Reanalysis for Research and Applications version 2 (MERRA-2). Drought conditions from the multi-LSM driven by multi-data set are useful to obtain the reliable information of land surface conditions. No land surface observations are sequentially assimilated into LSMs in the FLDAS. No predictions are carried out in the FLDAS so that the FLDAS is the pure monitoring system.

The advantage of our framework against the Princeton African Drought monitor and the FLDAS is that the LSM, EcoHydro-SiB, can directly simulate the vegetation condition (i.e., LAI) which is strongly correlated to the regional cereal production. Although the skill of the existing LSM to simulate vegetation dynamics is limited, we maximize the performance by assimilating satellite microwave observations into the LSM. Because vegetation dynamics has the better predictability (i.e., initial conditions are sometimes more important than the meteorological prediction) than the other land surface variables, we make it possible to predict vegetation dynamics in longer lead time (3 months). The disadvantage of our framework against the Princeton African Drought monitor and the FLDAS is that streamflow cannot be monitored and predicted since the LSM does not have any river routing schemes. In addition, while the Princeton African Drought monitor provides all information almost real time, our proposed framework needs the longer latency (see Section IV-D).

V. Conclusion

We applied the LDAS to monitor and predict agricultural droughts in North Africa. Our proposed monitoring framework can detect the historical nationwide crop failures in Morocco, Algeria, and Tunisia. The state-of-the-art seasonal meteorological prediction is useful to predict vegetation dynamics in 2–3-month lead time. We analyzed the predictability of vegetation dynamics using ESP and rESP and identified the importance of initial conditions compared to the meteorological forcings to predict LAI. Therefore, we can conclude that for agricultural drought prediction based on ecological variables, LDAS is not optional. It is extremely important to get the initial conditions of root-zone soil moistures and vegetation states by combining an LSM with observation data. We successfully provide a proof-of-concept numerical experiment for an operational agricultural drought monitoring and predicting system based on LDAS in North Africa. Since our proposed framework does not rely on any intensive *in situ* observation networks, it might be useful in the other ungauged regions.

Acknowledgment

The authors would like to thank the Japan Aerospace Exploration Agency (JAXA) for providing the AMSR-E brightness temperature data, Global Land Cover Facility for providing the GLASS LAI data, FAOSTAT for providing nationwide crop production data, the National Aeronautics and Space Administration (NASA) for providing GLDAS data, and the National Oceanic and Atmospheric Administration (NOAA) for providing the GFDL seasonal prediction ensembles. They would also like to thank T. R. McVicar for constructive comments to improve this article and three anonymous reviewers for their valuable comments.

References

[1] A. I. J. M. van Dijk *et al.*, "The Millennium Drought in southeast Australia (2001–2009): Natural and human causes and implications for water resources, ecosystems, economy, and society," *Water Resour. Res.*, vol. 49, pp. 1040–1057, Feb. 2013. doi: 10.1002/wrcr.20123.

[2] E. Boyd, R. J. Cornforth, P. J. Lamb, A. Tarhule, A. Brouder, and M. I. Lélé, "Building resilience to face recurring environmental crisis in African Sahel," *Nature Climate Change*, vol. 3, pp. 631–638, Jun. 2013. doi: 10.1038/NCLIMATE1856.

[3] R. Howitt, J. Melellín-Azuara, D. MacEwan, J. Lund, and D. Summer. (2014). *Economic Analysis of the 2014 Drought for California Agriculture*. [Online]. Available: http://www.circleofblue.org/wp-content/uploads/2014/07/Economic_Impact_of_the_2014_California_Water_Drought_0.pdf

[4] D. A. Wilhite, and M. H. Glantz, "Understanding: The drought phenomenon: The role of definitions," *Water Int.*, vol. 10, no. 3, pp. 111–120, 1985. doi: 10.1080/02508068508686328.

[5] Y. Sawada, T. Koike, and P. A. Jaranilla-Sanchez, "Modeling hydrologic and ecologic responses using a new eco-hydrological model for identification of droughts," *Water Resour. Res.*, vol. 50, pp. 6214–6235, Jul. 2014. doi: 10.1002/2013WR014847.

[6] X. Yuan and E. F. Wood, "Multimodel seasonal forecasting of global drought onset," *Geophys. Res. Lett.*, vol. 40, pp. 4900–4905, Sep. 2013. doi: 10.1002/grl.50949.

[7] A. W. Wood and D. P. Lettenmaier, "An ensemble approach for attribution of hydrologic prediction uncertainty," *Geophys. Res. Lett.*, vol. 35, Jul. 2008, Art. no. L14401. doi: 10.1029/2008GL034648.

[8] S. Shukla, J. Sheffield, E. F. Wood, and D. P. Lettenmaier, "On the sources of global land surface hydrologic predictability," *Hydrol. Earth Syst. Sci.*, vol. 17, pp. 2781–2796, Jul. 2013. doi: 10.5194/hess-17-2781-2013.

[9] J. Sheffield *et al.*, "A drought monitoring and forecasting system for Sub-Sahara African water resources and food security," *Bull. Amer. Meteorol. Soc.*, vol. 95, pp. 861–882, Jun. 2014. doi: 10.1175/BAMS-D-12-00124.1.

[10] A. McNally *et al.*, "A land data assimilation system for sub-Saharan Africa food and water security applications," *Sci. Data*, vol. 4, Feb. 2017, Art. no. 170012. doi: 10.1038/sdata.2017.12.

[11] M. Owe, R. D. Jeu, and J. Walker, "A methodology for surface soil moisture and vegetation optical depth retrieval using the microwave polarization difference index," *IEEE Trans. Geosci. Remote Sens.*, vol. 39, no. 8, pp. 1643–1654, Aug. 2001. doi: 10.1109/36.942542.

[12] H. Fujii, T. Koike, and K. Imaoka, "Improvement of the AMSR-E algorithm for soil moisture estimation by introducing a fractional vegetation coverage dataset derived from MODIS data," *J. Remote Sens. Soc. Jpn.*, vol. 29, no. 1, pp. 282–292, 2009.

[13] Y. Sawada, H. Tsutsui, and T. Koike, "Ground truth of passive microwave radiative transfer on vegetated land surfaces," *Remote Sens.*, vol. 9, no. 7, p. 655, 2017. doi: 10.3390/rs9070655.

[14] W. B. Anderson *et al.*, "Towards an integrated soil moisture drought monitor for East Africa," *Hydrol. Earth Syst. Sci.*, vol. 16, pp. 2893–2913, Aug. 2012. doi: 10.5194/hess-16-2893-2012.

[15] A. V. M. Ines, N. N. Das, J. W. Hansen, and E. G. Njoku, "Assimilation of remotely sensed soil moisture and vegetation with a crop simulation model for maize yield prediction," *Remote Sens. Environ.*, vol. 138, pp. 149–164, Nov. 2013. doi: 10.1016/j.rse.2013.07.018.

[16] P.-W. Liu *et al.*, "Assimilation of active and passive microwave observations for improved estimates of soil moisture and crop growth," *IEEE J. Sel. Topics Appl. Earth Observ. Remote Sens.*, vol. 9, no. 4, pp. 1357–1369, Apr. 2016. doi: 10.1109/JSTARS.2015.2506504.

[17] A. L. Barbu, J.-C. Calvet, J.-F. Mahfouf, and S. Lafont, "Integrating ASCAT surface soil moisture and GEOV1 leaf area index into the SURFEX modelling platform: A land data assimilation application over France," *Hydrol. Earth Syst. Sci.*, vol. 18, pp. 173–192, 2014. doi: 10.5194/hess-18-173-2014.

[18] Y. Sawada and T. Koike, "Simultaneous estimation of both hydrological and ecological parameters in an eco-hydrological model by assimilating microwave signal," *J. Geophys. Res., Atmos.*, vol. 119, no. 14, pp. 8839–8857, 2014. doi: 10.1002/2014JD021536.

[19] Y. Sawada, T. Koike, and J. P. Walker, "A land data assimilation system for simultaneous simulation of soil moisture and vegetation dynamics," *J. Geophys. Res., Atmos.*, vol. 120, pp. 5910–5930, Jun. 2015. doi: 10.1002/2014JD022895.

[20] S. Paloscia and P. Pampaloni, "Microwave polarization index for monitoring vegetation growth," *IEEE Trans. Geosci. Remote Sens.*, vol. GRS-26, no. 5, pp. 617–621, Sep. 1988. doi: 10.1109/36.7687.

[21] S. Paloscia and P. Pampaloni, "Microwave vegetation indexes for detecting biomass and water conditions of agricultural crops," *Remote Sens. Environ.*, vol. 40, pp. 15–26, Apr. 1992. doi: 10.1016/0034-4257(92)90123-2.

[22] Y. Sawada, T. Koike, K. Aida, K. Toride, and J. P. Walker, "Fusing microwave and optical satellite observations to simultaneously retrieve surface soil moisture, vegetation water content, and surface soil roughness," *IEEE Trans. Geosci. Remote Sens.*, vol. 55, no. 11, pp. 6195–6206, Nov. 2017. doi: 10.1109/TGRS.2017.2722468.

[23] L. A. Richards, "Capillary conduction of liquids through porous mediums," *J. Appl. Phys.*, vol. 1, no. 5, pp. 318–333, 1931. doi: 10.1063/1.1745010.

[24] M. T. van Genuchten, "A closed-form equation for predicting the hydraulic conductivity of unsaturated soils," *Soil Sci. Soc. Amer. J.*, vol. 44, no. 5, pp. 892–898, 1980.

[25] P. J. Sellers *et al.*, "A revised land surface parameterization (SiB_2) for atmospheric GCMS. Part I: Model formulation," *J. Climate*, vol. 9, no. 4, pp. 676–705, 1996.

[26] P. Friedlingstein, G. Joel, C. B. Field, and I. Y. Fung, "Toward an allocation scheme for global terrestrial carbon models," *Global Change Biol.*, vol. 5, pp. 755–770, Oct. 1999. doi: 10.1046/j.1365-2486.1999.00269.x.

[27] V. Y. Ivanov, R. L. Bras, and E. R. Vivoni, "Vegetation-hydrology dynamics in complex terrain of semiarid areas: 1. A mechanistic approach to modeling dynamic feedbacks," *Water Resour. Res.*, vol. 44, p. W03430, Mar. 2008. doi: 10.1029/2006WR005588.

[28] R. B. Jackson *et al.*, "A global analysis of root distributions for terrestrial biomes," *Oecologia*, vol. 108, pp. 389–411, Nov. 1996.

[29] J.-C. Calvet *et al.*, "An interactive vegetation SVAT model tested against data from six contrasting sites," *Agricult. Forest Meteorol.*, vol. 92, pp. 73–95, Jul. 1998.

[30] T. Mo, B. J. Choudhury, T. J. Schmugge, J. R. Wang, and T. J. Jackson, "A model for microwave emission from vegetation-covered fields," *J. Geophys. Res.*, vol. 87, pp. 11229–11237, Dec. 1982.

[31] T. J. Jackson and T. J. Schmugge, "Vegetation effects on the microwave emission of soils," *Remote Sens. Environ.*, vol. 36, no. 3, pp. 203–212, Jun. 1991. doi: 10.1016/0034-4257(91)90057-D.

[32] D. N. Kuria, T. Koike, H. Lu, H. Tsutsui, and T. Graf, "Field-supported verification and improvement of a passive microwave surface emission model for rough, bare, and wet soil surfaces by incorporating shadowing effects," *IEEE Trans. Geosci. Remote Sens.*, vol. 45, no. 5, pp. 1207–1216, May 2007.

[33] Q. Duan, S. Sorooshian, and V. Gupta, "Effective and efficient global optimization for conceptual rainfall-runoff models," *Water Resour. Res*, vol. 28, no. 4, pp. 1015–1031, 1992.

[34] S. Geman and D. E. McClure, "Statistical methods for tomographic image reconstruction," *Bull. Int. Statist. Inst.*, vol. 52, no. 4, pp. 5–21, 1987.

[35] Global Soil Data Task Group. (2000). *Global Gridded Surfaces of Selected Soil Characteristics (IGBPDIS)*. [Online]. Available: http://www.daac.ornl.gov/

[36] (2003). *Food and Agricultural Organization, Digital Soil Map of the World and Derived Soil Properties, Land Water Digital Media Ser. 1 [CR- ROM], Rome*. [Online]. Available: http://www.fao.org/ag/agl/lwdms.stm

[37] M. Kachi, K. Naoki, M. Hori, and K. Imaoka, "AMSR2 validation results," in *Proc. IEEE Int. Geosci. Remote Sens. Symp. (IGARSS)*, Jul. 2013, pp. 831–834. doi: 10.1109/IGARSS.2013.6721287.

[38] Z. Xiao *et al.*, "Use of general regression neural networks for generating the GLASS leaf area index product from time-series MODIS surface reflectance," *IEEE Trans. Geosci. Remote. Sens.*, vol. 52, no. 1, pp. 209–223, Jan. 2013. doi: 10.1109/TGRS.2013.2237780.

[39] M. Rodell *et al.*, "The global land data assimilation system," *Bull. Amer. Meteorol. Soc.*, vol. 85, no. 3, pp. 381–394, 2004.

[40] J. Sheffield, G. Goteti, and E. F. Wood, "Development of a 50-year high-resolution global dataset of meteorological forcings for land surface modeling," *J. Climate*, vol. 19, no. 13, pp. 3088–3111, 2006.

[41] G.-Y. Niu, Z.-L. Yang, R. E. Dickinson, L. E. Gulden, and H. Su, "Development of a simple groundwater model for use in climate models and evaluation with Gravity Recovery and Climate Experiment data," *J. Geophys. Res., Atmos.*, vol. 112, pp. 1–14, Apr. 2007. doi: 10.1029/2006JD007522.

[42] K. Yang *et al.*, "Auto-calibration system developed to assimilate AMSR-E data into a land surface model for estimating soil moisture and the surface energy budget," *J. Meteorol. Soc. Jpn.*, vol. 85A, pp. 229–242, Feb. 2007.

[43] R. Houborg, M. Rodell, B. Li, R. Reichle, and B. F. Zaitchik, "Drought indicators based on model-assimilated Gravity Recovery and Climate Experiment (GRACE) terrestrial water storage observations," *Water Resour. Res.*, vol. 48, Jul. 2012, Art. no. W07525. doi: 10.1029/2011WR011291.

[44] B. Li, D. Toll, X. Zhan, and B. Cosgrove, "Improving estimated soil moisture fields through assimilation of AMSR-E soil moisture retrievals with an ensemble Kalman filter and a mass conservation constraint," *Hydrol. Earth Syst. Sci.*, vol. 16, no. 1, pp. 105–119, 2012. doi: 10.5194/hess-16-105-2012.

[45] Y. Sawada and T. Koike, "Towards ecohydrological drought monitoring and prediction using a land data assimilation system: A case study on the Horn of Africa drought (2010–2011)," *J. Geophys. Res., Atmos.*, vol. 121, pp. 8229–8242, Jul. 2016. doi: 10.1002/2015JD024705.

[46] T. L. Delworth *et al.*, "Simulated climate and climate change in the GFDL CM2.5 high-resolution coupled climate model," *J. Climate*, vol. 25, no. 8, pp. 2755–2781, 2012. doi: 10.1175/JCLI-D-11-00316.1.

[47] B. P. Kirtman, D. Min, and J. M. Infanti, "The North American multimodel ensemble: Phase-1 seasonal-to-interannual prediction; phase-2 toward developing intraseasonal prediction," *Bull. Amer. Meteorol. Soc.*, vol. 95, pp. 585–601, 2014. doi: 10.1175/BAMS-D-12-00050.1.

[48] P. A. Jaranilla-Sanchez, L. Wang, and T. Koike, "Modeling the hydrologic responses of the Pampanga River basin, Philippines: A quantitative approach for identifying droughts," *Water Resour. Res.*, vol. 47, Mar. 2011, Art. no. W03514. doi: 10.1029/2010WR009702.

[49] L. Wang, T. Koike, K. Yang, and P. J.-F. Yeh, "Assessment of a distributed biosphere hydrological model against streamflow and MODIS Land Surface Temperature in the upper Tone River Basin," *J. Hydrol.*, vol. 377, pp. 21–34, Oct. 2009. doi: 10.1016/j.jhydrol.2009.08.005.

[50] J. Qin, S. Liang, K. Yang, I. Kaihotsu, R. Liu, and T. Koike, "Simultaneous estimation of both soil moisture and model parameters using particle filtering method through the assimilation of microwave signal," *J. Geophys. Res.*, vol. 114, Aug. 2009, Art. no. D15103. doi: 10.1029/2008JD011358.

[51] S. Madadgar, A. Aghakouchak, A. Farahmand, and S. J. Davis, "Probabilistic estimates of drought impacts on agricultural production," *Geophys. Res. Lett.*, vol. 44, pp. 7799–7807, Aug. 2017. doi: 10.1002/2017GL073606.

[52] L. Jarlan, G. Balsamo, S. Lafont, A. Beljaars, J. C. Calvet, and E. Mougin, "Analysis of leaf area index in the ECMWF land surface model and impact on latent heat and carbon fluxes: Application to West Africa," *J. Geophys. Res.*, vol. 113, Dec. 2008, Art. no. D24117. doi: 10.1029/2007JD009370.

[53] M. O. Jones, L. A. Jones, J. S. Kimball, and K. C. McDonald, "Satellite passive microwave remote sensing for monitoring global land surface phenology," *Remote Sens. Environ.*, vol. 115, pp. 1102–1114, Apr. 2011. doi: 10.1016/j.rse.2010.12.015.

[54] Y. Sawada and T. Koike, "Ecosystem resilience to the Millennium drought in southeast Australia (2001–2009)," *J. Geophys. Res. Biogeosci.*, vol. 121, pp. 2312–2327, Sep. 2016. doi: 10.1002/2016JG003356.

[55] T. J. Bohn, B. Livneh, J. W. Oyler, S. W. Running, B. Nijssen, and D. P. Lettenmaier, "Global evaluation of MTCLIM and related algorithms for forcing of ecological and hydrological models," *Agricult. Forest Meteorol.*, vol. 176, pp. 38–49, Jul. 2013. doi: 10.1016/j.agrformet.2013.03.003.

[56] X. Liang, D. P. Lettenmaier, E. F. Wood, and S. J. Burges, "A simple hydrologically based model of land surface water and energy fluxes for general circulation models," *J. Geophys. Res. Atmos.*, vol. 99, pp. 14415–14428, Jul. 1994. doi: 10.1029/94JD00483.

[57] G. J. Huffman, "The TRMM multisatellite precipitation analysis (TMPA): Quasi-global, multiyear, combined-sensor precipitation estimates at fine scales," *J. Hydrometeorol.*, vol. 8, no. 1, pp. 38–55, 2007. doi: 10.1175/JHM560.1.

[58] M. B. Ek *et al.*, "Implementation of Noah land surface model advances in the National Centers for Environmental Prediction operational mesoscale Eta model," *J. Geophys. Res.*, vol. 108, p. 8851, Nov. 2003. doi: 10.1029/2002JD003296.
[59] P. Xie and P. Arkin, "Global precipitation: A 17-year monthly analysis based on gauge observations, satellite estimates, and numerical model outputs," *Bull. Amer. Meteorol. Soc.*, vol. 78, no. 11, pp. 2539–2558, 1997. doi: 10.1175/1520-0477(1997)078<2539:GPAYMA>2.0.CO;2.
[60] C. Funk *et al.*, "The climate hazards infrared precipitation with stations—A new environmental record for monitoring extremes," *Sci. Data*, vol. 2, Dec. 2015, Art. no. 150066. doi: 10.1038/sdata.2015.66.

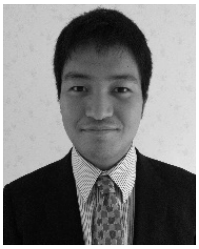

Yohei Sawada received the B.Eng., M.Eng, and the Ph.D. degrees from The University of Tokyo, Tokyo, Japan, in 2011, 2013, and 2016, respectively.

He was a Post-Doctoral Researcher with the RIKEN Advanced Institute for Computational Science, Kobe, Japan, and a Researcher with the Meteorological Research Institute, Japan Meteorological Agency, Tokyo, Japan. He is currently an Associate Professor with The University of Tokyo, Tokyo. His research interests include data assimilation, microwave remote sensing, and hydrometeorological disaster monitoring and prediction.

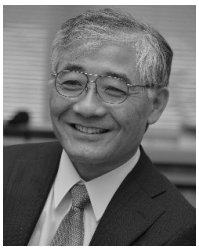

Toshio Koike received the bachelor's and master's degrees and doctor of engineering from The University of Tokyo, Tokyo, Japan, in 1980, 1982, and 1985, respectively.

He joined The University of Tokyo as a Research Associate in 1985, where he was a Lecturer from 1986 to 1987. He was an Associate Professor with the Nagaoka University of Technology, Nagaoka, Japan, from 1988 to 1999, where he was a Professor in 1999. In 1999, he joined the Department of Civil Engineering, The University of Tokyo, where he held the position of Professor till 2017. He is currently the Executive Director with the International Centre for Water Hazard and Risk Management (ICHARM), Tsukuba, Japan, under the auspices of UNESCO, and a Professor Emeritus with The University of Tokyo.

Dr. Koike has been a Chair with the River Council of Japan since 2015 and led discussions on important river-related matters to advise the Minister of Land, Infrastructure, Transport, and Tourism of Japan. In his capacity as a Council Member of the Science Council of Japan, Cabinet Office, he has also helped to improve and develop various aspects of science nationwide since 2017 via the provision of policy recommendations to the government and the public.

Eiji Ikoma received the B.E. degree in electronics engineering and the Ph.D. degree in electrical engineering and information systems from The University of Tokyo, Tokyo, Japan, in 1995 and 2000, respectively.

In 2000, he joined the Institute of Industrial Science, The University of Tokyo, as a Researcher. From 2003 to 2008, he was an Associate Researcher with the Center for Spatial Information, and from 2009 to 2012, with the Earth Observation Data Integration and Fusion Research Initiative (EDITORIA), The University of Tokyo. He accepted the position of Project Associate Professor at EDITORIA in 2010. He started to join the project "DIAS" from the beginning of its first term 2006, and proceed the research about database and user interface system with members of Information Technology Team on DIAS project, and he is currently a Core Member of the DIAS Platform Development Group. Since 2016, he has been a Senior Scientific Research Specialist of Ministry of Education, Culture, Sports, Science and Technology, Japan.

Masaru Kitsuregawa (F'12) received the Ph.D. degree from The University of Tokyo, Tokyo, Japan, in 1983.

He is currently the Director General with the National Institute of Informatics and a Professor with the Institute of Industrial Science, The University of Tokyo. His research interests include database engineering.

Dr. Kitsuregawa is a fellow of ACM, IEICE, and IPSJ. He received many awards including the ACM SIGMOD E. F. Codd Innovations Award, the IEICE Achievement Award, the IPSJ Contribution Award, the 21st Century Invention Award of National Commendation for Invention, Japan, and the C&C Prize. In 2013, he awarded Medal with Purple Ribbon and in 2016, the Chevalier de la Legion D'Honneur. He served various positions such as President of Information Processing Society of Japan from 2013 to 2015 and the Chairman of the Committee for Informatics, Science Council of Japan from 2014 to 2016.